KVN Status Report 2025

Korean VLBI Network,
Korea Astronomy and Space Science Institute

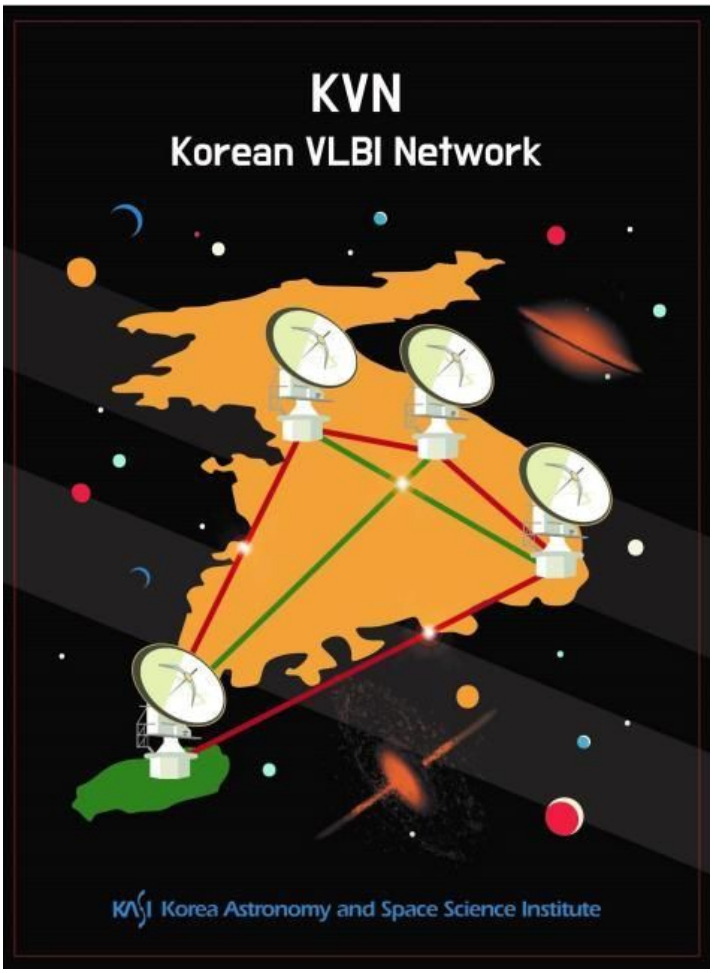

June 02, 2025
Center for KVN

Contents

List of Tables

List of Figures

1 Introduction

The Korean VLBI Network (KVN) is a Very Long Baseline Interferometry (VLBI) facility in Korea that operates at millimeter wavelengths. It consists of four 21-m radio telescopes located in Seoul (Yonsei University), Ulsan (University of Ulsan), Jeju, and Pyeongchang (newly constructed on the Pyeongchang campus of Seoul National University). This network offers a comparable spatial resolution to a radio telescope spanning about 500 km (see Figure 1). However, it is considered a relatively modest network when compared to the larger American and European VLBI networks, such as the Very Long Baseline Array (VLBA) and the European VLBI Network (EVN). To address this limitation, KASI has developed innovative multi-frequency band receiver systems that simultaneously observe four different frequencies: K, Q, W, and D bands (with center frequencies of 22, 43, 86, and 129 GHz). In August 2013, a C band (6 GHz) receiver was installed on the KVN Ulsan radio telescope, which was operating in VLBI mode with the East Asia VLBI Network (EAVN) telescopes. The installation of GPS receivers at each KVN station has significantly improved the precision of phase referencing and astrometric observations. This enhancement is due to the ability of the GPS receivers to estimate atmospheric wet delays and total electron content, both of which are critical parameters for the KVN stations. Moreover, the newly built Pyeongchang Telescope has expanded its observational capabilities to cover the 230 GHz band. Since May 2025, the Pyeongchang Telescope has also been enhanced with CX, and Ka band (6 – 9 and 28 – 34 GHz) receivers in order to maximize its efficiency and performance.

This remarkable capability enables the KVN to study the formation and evolutionary processes of stars, the structure and dynamics of our galaxy, the nature of active galactic nuclei, and more, with milli-arcsecond resolution [1]. By employing such advanced technology, we have demonstrated its commitment to pushing the boundaries of scientific research and fostering collaboration among experts in the field.

2 KVN System

2.1 Network

2.1.1 Array

The KVN is a four-component VLBI network in South Korea dedicated to millimeter-wavelength VLBI observations. Four 21-m radio telescopes are strategically positioned in Seoul, Ulsan, Jeju, and Pyeongchang, respectively: each is the KVN Yonsei Radio Telescope (hereafter KYS), the KVN Ulsan Radio Telescope (hereafter KUS), the KVN Tamna Radio Telescope (hereafter KTN), and the KVN Pyeongchang Radio Telescope (hereafter KPC). The baseline lengths of these telescopes span from 133 to 478 km. All these antennas share an identical design, ensuring uniformity in their capabilities and performance (see Figure 2).

2.1.2 UV coverage

Figure 3 presents the simulated UV coverage of the KVN at K band for sources with varying declination (+60°, +30°, 0°, and −30°) observed over 12 hours.

Figure 1: The location of the Korean VLBI Network (KVN).

2.1.3 Antenna location

Table 1 presents the coordinates of KVN antennas, while Table 2 shows the geometric locations of the four KVN stations. The position of all antennas has been determined using GPS, and KVN antenna positions are routinely monitored by GPS and geodetic VLBI observations in collaboration with VLBI Exploration of Radio Astrometry (VERA) of Japan.

2.1.4 Array Operation Center (AOC)

KVN antennas can be remotely controlled by the Array Operation Center (AOC) at the East Asia VLBI Center, KASI, Daejeon. KVN stations are interconnected with the AOC by a high-speed dedicated network called KREONET (Korea Research Environment Open NETwork). Considering the KVN antennas can be controlled remotely from the AOC, it

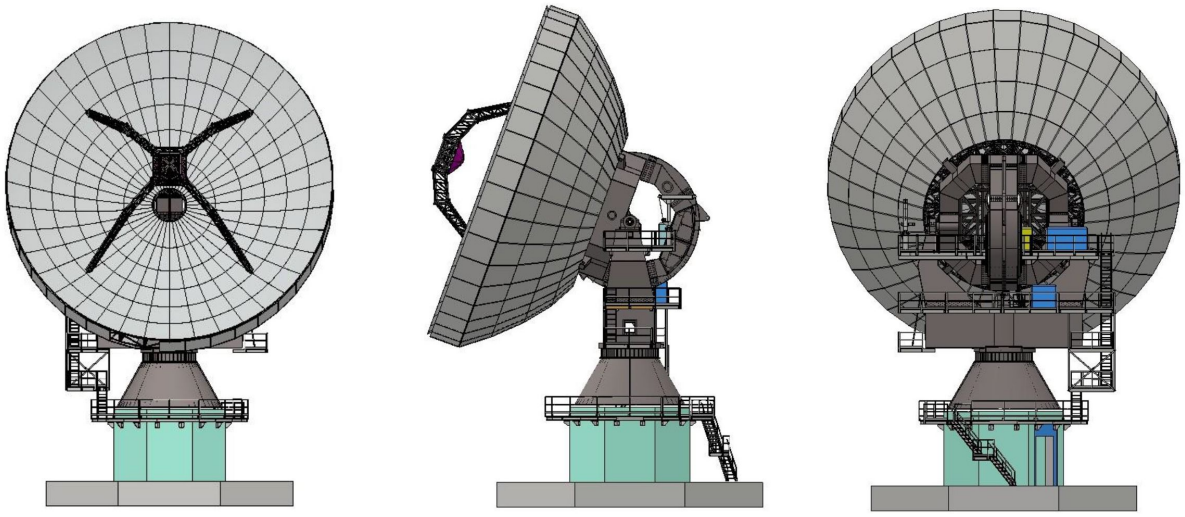

Figure 2: Design of the KVN antenna.

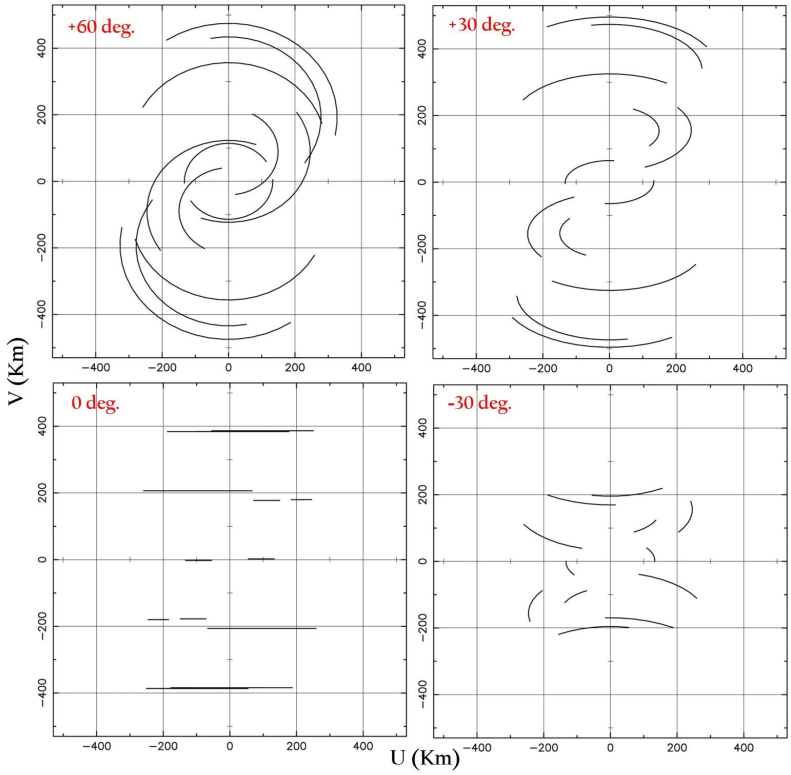

Figure 3: UV coverage simulation for the K band.

is vital that the AOC operator is aware of the weather conditions that can influence the quality of the VLBI data. Each KVN antenna has its own weather station that transmits information on air temperature, dew point, wind speed, wind direction, and air pressure to the AOC.

Table 1: The geographical locations of the KVN antennas

Antenna	Longitude (° ′ ″)	Latitude (° ′ ″)	Altitude (m)
KYS	126:56:27.4	37:33:54.9	139
KUS	129:14:59.3	35:32:44.2	170
KTN	126:27:34.4	33:17:20.9	452
KPC	128:26:55.1	37:32:00.1	557

Table 2: [a]Positions of KVN antennas by IVP measurement using GNSS

Antenna	Epoch	X (m)	Y (m)	Z (m)
KYS	May 08, 2024	−3042281.1397	4045902.5831	3867374.2657
KUS	May 08, 2024	−3287268.7693	4023450.0547	3687379.9226
KTN	Feb. 23, 2023	−3171731.7786	4292678.4406	3481038.7157
KPC	May 08, 2024	−3149228.7801	3966414.5295	3864840.1629

[a] *The positional solution was developed on December 24, 2024, utilizing over 2,500 IVS R1R4 sessions and more than 10 EAVN sessions.*

2.2 Antennas

2.2.1 Optics and Driving performance

The KVN antennas are shaped Cassegrain-type antennas featuring altitude-azimuth mounts. The main reflector has a diameter of 21-m and a focal length of 6.78-m. Comprising 200 aluminum panels, the main reflector achieves a manufacturing surface accuracy of approximately 65 μm. The main reflector can move at a speed of 3°/second, facilitating fast position-switching observations. The position, tilt and tip of the sub-reflector are remotely controlled and modeled to account for the effects of gravitational deformation on the main reflector and sagging of the sub-reflector. Furthermore, the newly constructed KPC antennas perform slightly better than the old KVN antennas. For further details on the antenna optics, kindly refer to Table 3.

2.2.2 Gain Curve

The main reflector panels of KVN antennas were installed to give the maximum gain at the elevation angle of $\sim 48°$. The sagging of the sub-reflector and the deformation of the main reflector by gravity with elevation results in degradation of antenna aperture efficiency with elevation. To compensate for this effect, a hexapod is utilized to adjust the sub-reflector position in KVN antennas. Although the hexapod correction reduces significantly the dependence of aperture efficiency with elevation, the degradation still appears evidently at a higher frequency. By tracking strong maser sources or planets such as Jupiter or Mars at different altitudes, we can measure how the efficiency of the antenna changes relative to elevation. The gain curve measurements for the KYN, KUS, and KTN were conducted on December 24 and 23, 2023, and May 3, 2022, respectively. The KPC's measurements were taken on February 14 of this year, utilizing the newly installed Compact Triple-band

Table 3: Specification of KVN antennas

Main reflector (Axisymmetric Paraboloid)	Parameters
Diameter	D = 21.03 m
Focal length	f ≈ 6.78 m
Focal ratio	f/D = 0.32
Panels manufacturing accuracy	65 μm (KVN), ≤ 60 μm (KPC)
Alignment surface accuracy	54 μm (KVN), ≤ 50 μm (KPC)
Sub-reflector (Hyperboloid)	**Parameters**
Diameter	d ≈ 2.25 m
Manufacturing surface accuracy	50 μm (KVN), ≤ 30 μm (KPC)
Expected total surface accuracy	124 μm at EL 48°
Panel	73 μm
Alignment	60 μm
Subreflector	52 μm
Backup structure	62 μm
Slewing speed	3 °/sec
Slewing acceleration	3 °/sec^2
Operating range	Az.: $-90° \sim +450°$, El.: $0° \sim 90°$

Receiver (a.k.a., CTR) to achieve more precise gain curve measurements than previously possible. Figure 4 shows the elevation dependency of antenna gain of all four radio telescopes measured by observing several strong sources, Mars, Jupiter, Mira variables TX Cam, U Her, and AGN 3C 84, utilizing the observation mode of "Five pointing" and "Cross Scan". The W-low and W-high bands measured for the KPC correspond to frequencies of 86 GHz and 112 GHz, respectively. Additionally, a 150/230 GHz receiver is planned to be installed on the KPC in 2025.

We derived a normalized gain curve which has the following form: $G\_norm = A0 \cdot EL^2 + A1 \cdot EL + A2$, where EL is the elevation in degree, by fitting a second-order polynomial to the data and normalizing the fitted function with its maximum value. The fitted parameters are summarized in Table 4. The values displayed in Table 4 represent the average of Left Circular Polarization (LCP) and Right Circular Polarization (RCP).

2.2.3 Antenna beam size and Aperture efficiency

Between December 2021 and March 2022, main reflector panel alignments (using photogrammetry) were carried out on three existing KVN antennas. In March 2024, an additional panel alignment was performed on the KYS antenna, and the sub-reflector was replaced. Furthermore, the measurement of the primary mirror panels for the recently constructed KPC antenna was completed in March 2024. Accordingly, the surface accuracies of four KVN telescopes were enhanced to 52 (KYS), 72 (KUS), 70 (KTN), and 55 (KPC) μm, respectively. Furthermore, the KVN system was recently upgraded to a wide-band receiving system employing a new sampler, the OCTAD, encompassing the frequency ranges of 18–26 GHz (K), 35–50 GHz (Q), 85–116 GHz (W), and 125–142 GHz (D), respectively (see

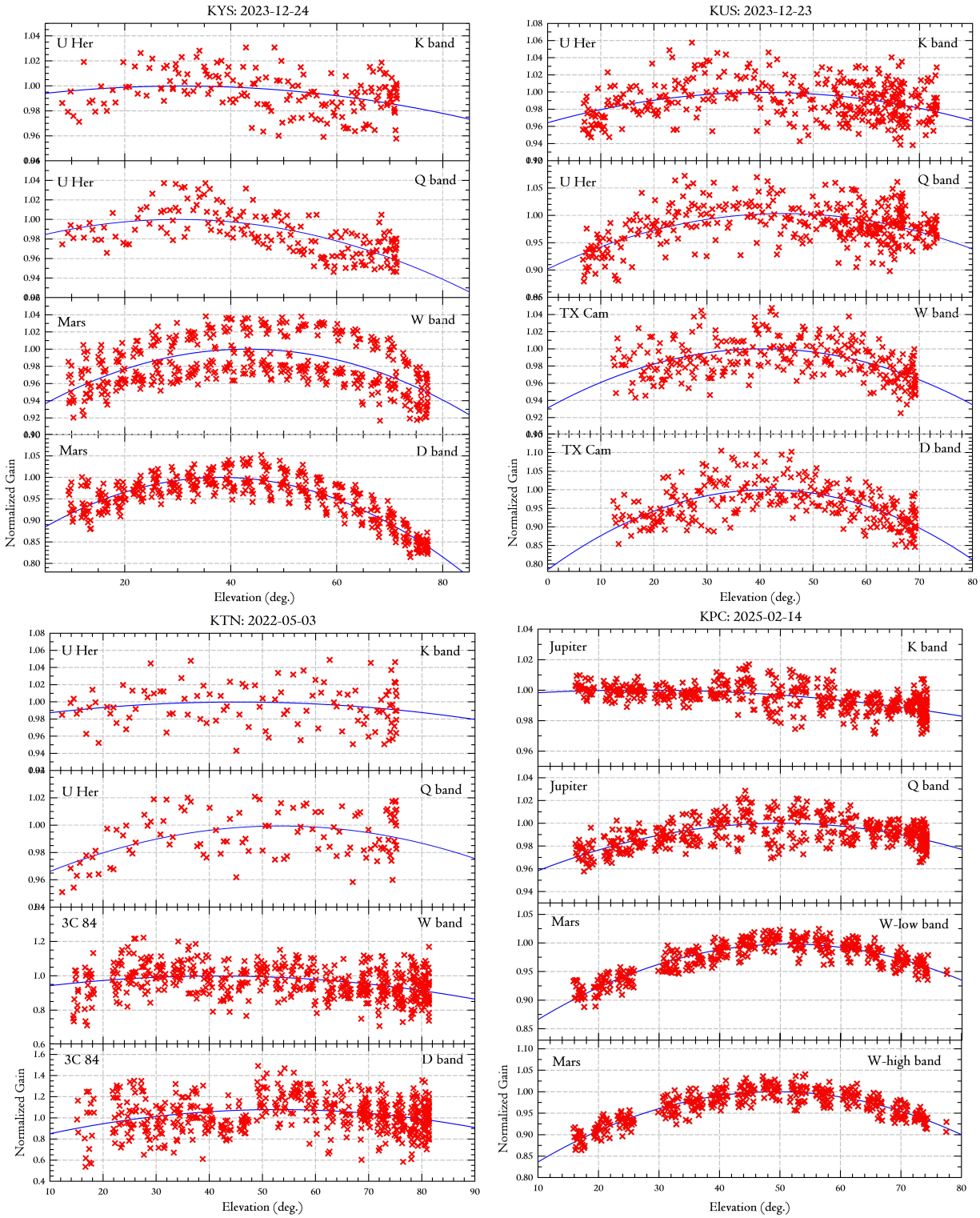

Figure 4: Gain curves of K- (22), Q- (43), W- (86), and D- (129 GHz) bands at each KVN antenna. The W-low and W-high bands in KPC correspond to 86 GHz and 112 GHz, respectively.

Table 4: Coefficients of normalized gain curves (the average of LCP and RCP)

Station	Reference Freq.	A0	A1	A2
KYS	22	−8.9467E−06	5.4653E−04	9.9150E−01
	43	−2.4528E−05	1.4734E−03	9.7785E−01
	86	−5.6926E−05	4.7124E−03	9.0124E−01
	129	−1.5973E−04	1.3696E−02	7.0643E−01
KUS	22	−1.9115E−05	1.4894E−03	9.7040E−01
	43	−5.1311E−05	4.5593E−03	9.0199E−01
	86	−3.8227E−05	3.1453E−03	9.3526E−01
	129	−1.2589E−04	1.0413E−02	7.8466E−01
KTN	22	−1.0840E−05	9.6959E−04	9.7824E−01
	43	−1.6814E−05	1.7814E−03	9.5205E−01
	86	−5.6926E−05	4.7124E−03	9.0124E−01
	129	−1.1899E−04	1.2518E−02	7.4806E−01
KPC	22	−6.0758E−06	3.2594E−04	9.9568E−01
	43	−2.5878E−05	2.5952E−03	9.3493E−01
	86	−7.7221E−05	7.9288E−03	7.9452E−01
	112	**−1.0597E−04**	**1.0447E−02**	**7.4254E−01**

Section 2.3). Therefore, in all wide K, Q, W, and D bands, we measured HPBW, aperture efficiency, and main-beam efficiency using the OCTAD. However, the KPC has not yet been fully set up with OCTAD, so limited measurements have been made at K, Q, and W bands.

The results are shown in Table 5 as representative values for each band. While the W and D band values were acquired through observations toward Mars and Uranus, the K and Q band values were obtained through observations toward Jupiter. The brightness temperatures for Jupiter in the K and Q bands are applied from de Pater et al. (2019)[2] and Maris et al. (2021)[3]. The estimates for the W and D bands use the Mars brightness modeling data that are displayed on its website[1]. Figure 5 displays the efficiency and beam size for each band of the telescopes.

- **Elevation dependency**
  With elevation, aperture efficiency changes. The previous section provided the gain curve that depicts the elevation dependency of the KVN antennas. The maximum values are those listed in Column (4).

- **Frequency dependency of beam efficiency**
  Beam efficiency also varies with beam size. The measured HPBWs are tabulated in Column (3), which are almost the same as the theoretical one (= λ/D of the antenna). To get a beam efficiency at 90 GHz, you have to multiply $(86/90)^2$ to that at 86 GHz.

- **Quantization correction of single-dish spectrum data**
  Prior to performing efficiency adaptations, single-dish spectrum data must be multi-

[1] https://lesia.obspm.fr/perso/emmanuel-lellouch/mars/

Table 5: Beam size, efficiencies, and DPFU[a] of each KVN antenna

Site	Frequency (Band) (GHz)	HPBW (arcsec)	η_A (%)	η_B (%)	DPFU (K/Jy)
(1)	(2)	(3)	(4)	(5)	(6)
KYS	22 (K)	130	68	58	0.0858
	40 (Q-low)	73	70	60	0.0876
	43 (Q-high)	66	75	62	0.0936
	47 (Q-high)	64	71	60	0.0887
	86 (W-low)	32	57	43	0.0712
	95 (W-low)	30	46	38	0.0572
	103 (W-high)	28	46	39	0.0582
	111 (W-high)	27	46	40	0.0572
	129 (D)	25	36	34	0.0450
	140 (D)	24	31	35	0.0387
KUS	22 (K)	127	73	60	0.0920
	40 (Q-low)	72	68	58	0.0855
	43 (Q-high)	65	70	57	0.0876
	47 (Q-high)	61	66	57	0.0833
	86 (W-low)	32	63	47	0.0786
	95 (W-low)	29	58	45	0.0723
	103 (W-high)	27	56	45	0.0698
	111 (W-high)	26	55	47	0.0685
	129 (D)	23	53	47	0.0667
	140 (D)	21	42	38	0.0521
KTN	22 (K)	131	71	62	0.0894
	40 (Q-low)	70	68	54	0.0847
	43 (Q-high)	63	66	50	0.0825
	47 (Q-high)	58	64	48	0.0804
	86 (W-low)	35	52	48	0.0656
	95 (W-low)	28	54	38	0.0674
	103 (W-high)	27	50	41	0.0633
	111 (W-high)	26	52	44	0.0652
	129 (D)	22	39	32	0.0485
	140 (D)	21	34	29	0.0428
KPC	22 (K)	135	78	63	0.0983
	43 (Q)	66	71	65	0.0887
	86 (W-low)	34	68	59	0.0856
	111 (W-high)	26	58	49	0.0727

[a] indicates the Degree Per Flux density Unit.
η_A: Aperture efficiency, η_B: Main-beam efficiency.

plied by a factor of 1.25 if it is being reduced. This is to compensate for the effects of the digital filter and spectrometer.

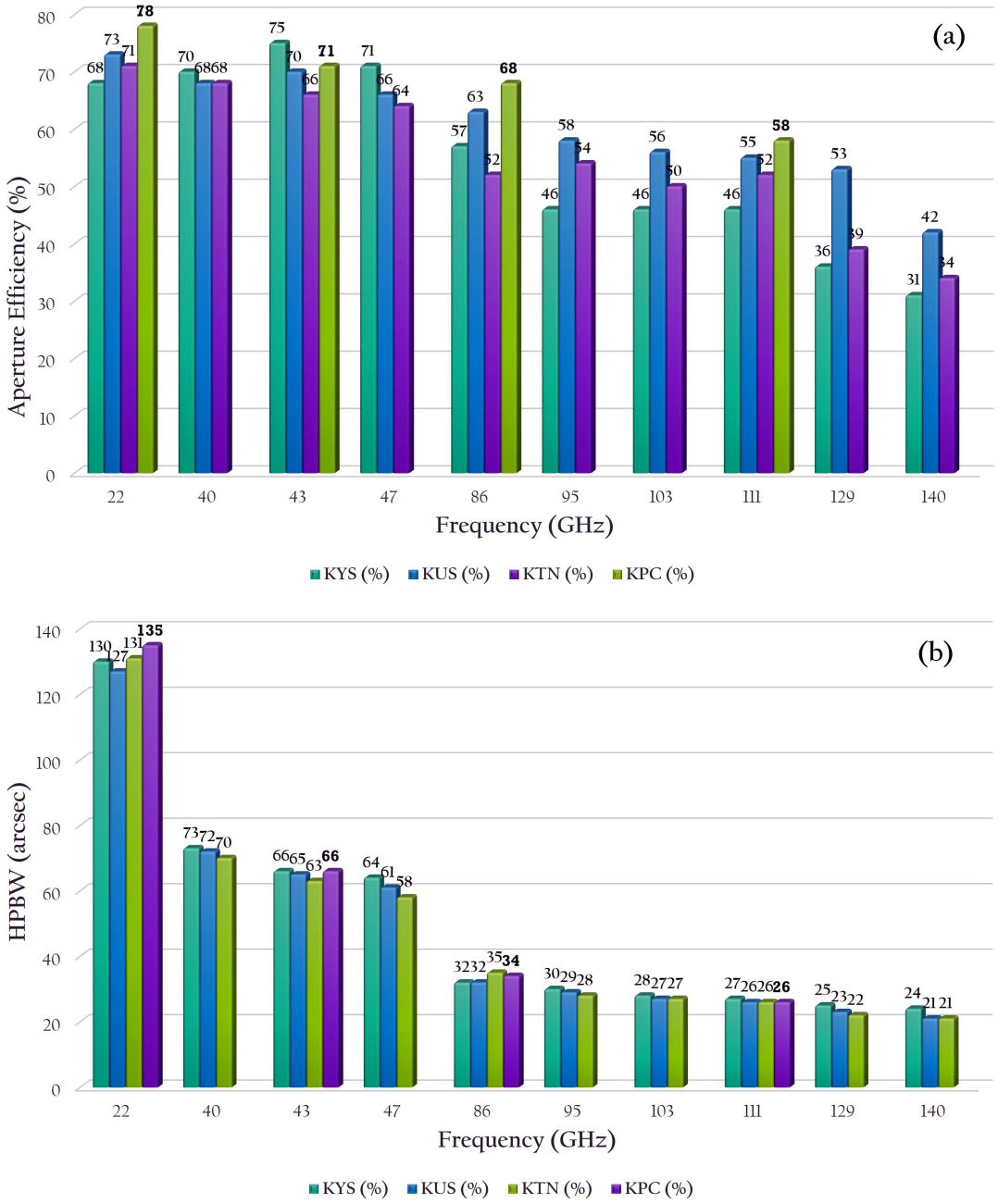

Figure 5: Aperture efficiencies and HPBWs of four KVN telescopes. (a): Aperture efficiency, (b) HPBW.

- Parameters of Table 5 can be applied for the following observing season;
  - KYS: from December 2024 – now
  - KUS: from December 2024 – now
  - KTN: from November 2024 – now
  - KPC: from February 2025 – now

2.2.4 Beam pattern

The KVN antenna optics are of the shaped-Cassegrain type, with a main reflector and sub-reflector designed to provide uniform illumination on an aperture plane. This design allows for greater aperture efficiency compared to conventional Cassegrain-type antennas. However, it should be noted that it also results in a higher sidelobe level, which may need to be taken into consideration. Figure 6 displays On-The-Fly (OTF) images of Venus and Jupiter at 86 GHz and 129 GHz, and 22 GHz and 43 GHz, respectively, as measured using the KYS antenna. The map size is $12' \times 10'$ for 22 and 43 GHz, and $3.5' \times 3'$ for 86 and 129 GHz. The first sidelobe pattern is visible. It is worth noting that KVN antennas typically exhibit sidelobe levels of -14 to -13 dB.

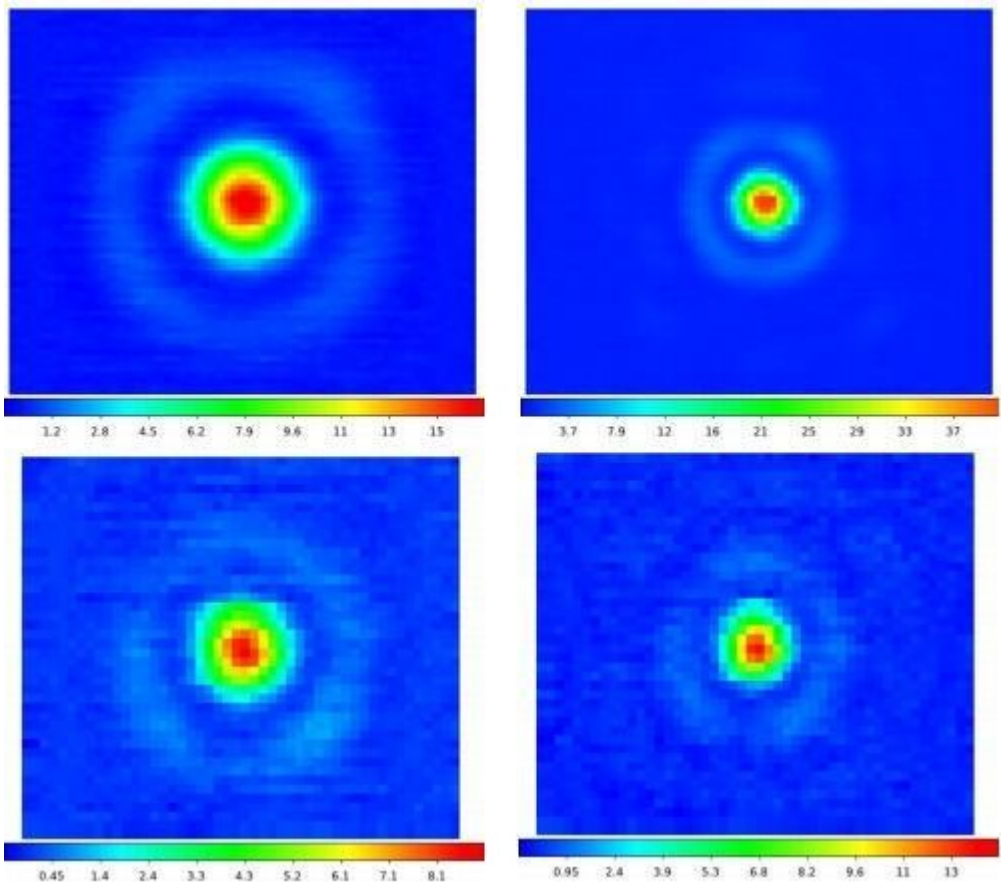

Figure 6: Beam patterns at the KYS antenna. Top panels: Jupiter at 22 GHz (left) and 43 GHz (right), Bottom panels: Venus at 86 GHz (left) and 129 GHz (right).

2.2.5 Antenna pointing accuracy

There can be systematic differences between the direction a radio telescope is intended to point and the direction it actually points. These differences can be caused by factors such as errors resulting from the telescope axis not being aligned with the true altitude-azimuth axis, deviations due to warped bearing planes, deviations due to gravitational deformation, and

deviations due to non-ideal telescope construction. These systematic and recurring orientation errors are often expressed as a function of altitude and azimuth. The pointing model offers values for these errors based on altitude and azimuth to make necessary adjustments.

The KVN antenna aims for an accuracy of 4 arcseconds. In order to achieve and sustain this level of precision, periodic observations are taken to construct a pointing model. The equations of the pointing model for the KVN are given below:

$$\begin{aligned}\Delta\mathrm{A} &= \mathrm{IA} + \mathrm{CA}\ \sec(\mathrm{E}) + \mathrm{NPAE}\ \tan(\mathrm{E}) + \mathrm{AN}\ \tan(\mathrm{E})\ \sin(\mathrm{A}) - \mathrm{AW}\ \tan(\mathrm{E})\ \cos(\mathrm{A}) \\ &\quad + \mathrm{WA1}\ \tan(\mathrm{E})\ \sin(2\mathrm{A}) + \mathrm{WA2}\ \tan(\mathrm{E})\ \cos(2\mathrm{A}) + \mathrm{Aobs}\ \sec(\mathrm{E}) \\ \Delta\mathrm{E} &= \mathrm{IE} + \mathrm{GF}\ \cos(\mathrm{E}) + \mathrm{GF2}\ \sin(\mathrm{E}) + \mathrm{AN}\ \cos(\mathrm{A}) + \mathrm{AW}\ \sin(\mathrm{A}) + \mathrm{WA1}\ \cos(2\mathrm{A}) \\ &\quad + \mathrm{WA2}\ \sin(2\mathrm{A}) + \mathrm{R(Ps, Ts, RH, E)} + \mathrm{ERC}\ \cot(\mathrm{E}) + \mathrm{Eobs}\end{aligned}$$

In the above equation, IA = Az encoder zero offset, CA = Collimation error of RF axis, NPAE = Non-perpendicularity between Az & El axes, AN = Az axis misalignment in N-S, AW = Az axis misalignment in E-W, WA1 & WA2 = Azimuth bearing warp, Aobs = Az pointing offset, IE = El encoder zero offset, GF = Gravitational flexure correction at horizon, GF2 = Gravitational flexure correction for mis-centered EL drive and encoder system, ERC = Empirical correction for atmospheric refraction, Elobs = El pointing offset, and R(Ps,Ts,RH,E) = Refractive index of the atmosphere, where Ps, Ts, and RH = barometric pressure, temperature, and relative humidity, respectively.

Another factor that affects pointing accuracy is the impact of temperature differences in the antenna structure. This factor is challenging to incorporate into a basic pointing model due to its complex nature, which is influenced by variables such as the variance between the sun and antenna orientation, temperature differentials, and other factors. It is known that the temperature difference between the antenna yoke and pedestal has a significant effect on the pointing of the antenna. KVN has designed the antenna in a way that ensures the temperature difference between these parts is maintained below 1 degree (KVN-21M Technical Memo 136, 152). However, actual measurements have shown that the pointing is off by up to 10 seconds per hour during the day when the sun is shining. Therefore, it is necessary to make pointing observations at least every 2 hours during the day, especially at sunrise and sunset, in order to maintain the pointing accuracy at less than 6 arcseconds root mean square.

Since 2009, the telescope's pointing accuracy has been measured using a sample of evolved stars (mainly, 43 GHz SiO maser line). Table 6 presents the pointing accuracy of the four KVN telescopes that were measured in January and February, 2025. Table 6 provides the total, azimuth, and elevation of the root mean square (rms) of the residual pointing offsets between the observations and the pointing models for each epoch and telescope, accordingly (Total Error = $Sqrt(Az\_Error^2 + El\_Error^2)$. Figure 7 displays the residuals of each KVN telescope's pointing model.

2.2.6 Beam alignment

The KVN is distinguished by its unique ability to observe a specific target object using four frequency bands simultaneously, a capability unmatched by any other radio observing

Table 6: KVN Antenna Pointing Accuracy

Site	Total (arcsec)	Azimuth (arcsec)	Elevation (arcsec)	Frequency (GHz)	Date
KYS	**2.76**	1.41	2.37	43	January 29, 2025
KUS	**4.33**	2.89	3.22	43	January 27, 2025
KTN	**4.61**	2.96	3.53	43	January 24, 2025
KPC	**2.75**	1.42	2.36	43	February 12, 2025

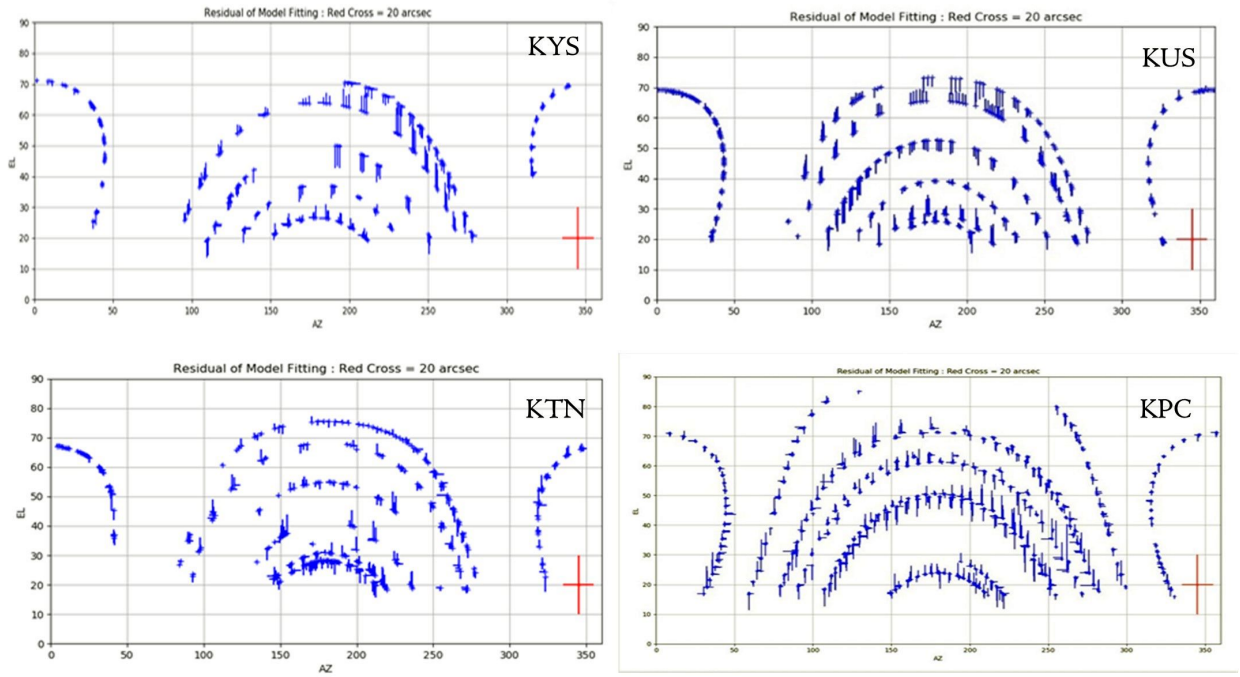

Figure 7: The residual of pointing models (KYS, KUS, KTN, and KPC from top-left to bottom-right).

system in the world. Consequently, the KVN's quasi-optical system must be calibrated so that each of the four beams is directed at the same point in the sky, facilitating simultaneous observation across all four frequency bands. To achieve this, the 86 GHz RCP beam was used as a reference point, and the position of the quasi-optical system was adjusted to ensure that the beams of the other frequency bands were properly aligned with its center point. The pointing offset values were subsequently analyzed. The receiver installed on the KPC differs from those on previous KVN telescopes due to its incorporation of CTRs in the 22, 43, and 86 GHz bands. Notably, the 22 and 43 GHz beams are aligned with respect to the LCP beam at 86 GHz. The results of this measurement are summarized in Table 7.

2.2.7 Skylines

Skylines are the limits of the viewable height with azimuth below which we cannot see the sky. These limits are determined by obstructions caused by the neighboring buildings,

Table 7: AZ/EL beam offset with respect to the 86 GHz RCP beam

Site	Band (L, R) (GHz)	Az. offset (arcsec)	El. offset (arcsec)	Measeured Date
KYS	22 (L)	+0.2 (±0.1)	+2.2 (±0.1)	February 02, 2024
	22 (R)	+1.0 (±0.2)	+1.9 (±0.2)	February 02, 2024
	43 (L)	+1.2 (±0.3)	+0.8 (±0.2)	February 02, 2024
	43 (R)	+2.9 (±0.4)	+0.8 (±0.3)	February 02, 2024
	86 (L)	−2.1 (±0.1)	−0.1 (±0.1)	December 10, 2024
	86 (R)			December 10, 2024
	129 (L)	+0.1 (±0.5)	−1.6 (±0.5)	December 10, 2024
	129 (R)	−1.2 (±0.4)	+2.1 (±0.7)	December 10, 2024
KUS	22 (L)	−0.8 (±0.5)	+2.0 (±0.6)	September 30, 2021
	22 (R)	−1.6 (±1.4)	+3.1 (±0.1)	September 30, 2021
	43 (L)	−0.5 (±0.2)	+0.4 (±0.1)	September 30, 2021
	43 (R)	−1.0 (±0.0)	+0.3 (±0.0)	September 30, 2021
	86 (L)	−1.4 (±0.1)	−0.1 (±0.1)	September 30, 2021
	86 (R)			September 30, 2021
	129 (L)	−1.0 (±0.2)	+1.5 (±0.3)	September 30, 2021
	129 (R)	−1.3 (±0.1)	+1.1 (±0.4)	September 30, 2021
KTN	22 (L)	+1.0 (±0.1)	−2.0 (±0.1)	August 19, 2024
	22 (R)	−2.0 (±0.2)	−1.0 (±0.2)	August 19, 2024
	43 (L)	−2.0 (±0.1)	−2.0 (±0.1)	August 19, 2024
	43 (R)	+0.5 (±0.1)	−0.6 (±0.1)	August 19, 2024
	86 (L)	+1.0 (±0.1)	−2.0 (±0.1)	August 19, 2024
	86 (R)			August 19, 2024
	129 (L)	+1.9 (±0.2)	+0.4 (±0.1)	August 19, 2024
	129 (R)	+0.9 (±0.1)	+1.4 (±0.1)	August 19, 2024
KPC	22 (L)	+0.3 (±0.2)	+1.3 (±0.2)	April 02, 2024
	43 (L)	+1.5 (±0.2)	−0.1 (±0.2)	April 02, 2024
	86 (L)			April 02, 2024

trees, and mountains. Skylines of KVN sites measured in May 2025 are shown in Figure 8.

2.3 Receiver

2.3.1 Quasi-optics

The KVN has the unique capability to observe four frequency bands [4], [5], simultaneously. KVN quasi-optics were designed to enable this multi-frequency observation. Figure 9 shows the layout of quasi-optics and receivers viewing from the sub-reflector side. The quasi-optics system splits one signal from the sub-reflector into four using three dichroic low-pass filters marked as LPF1, LPF2, and LPF3 in Figure 9. The split signals into four different frequency bands are guided to corresponding receivers.

In mid-2023, the construction of the KPC was completed. It has been conducting test

Figure 8: Skylines of KYS, KUS, KTN, and KPC from top to bottom.

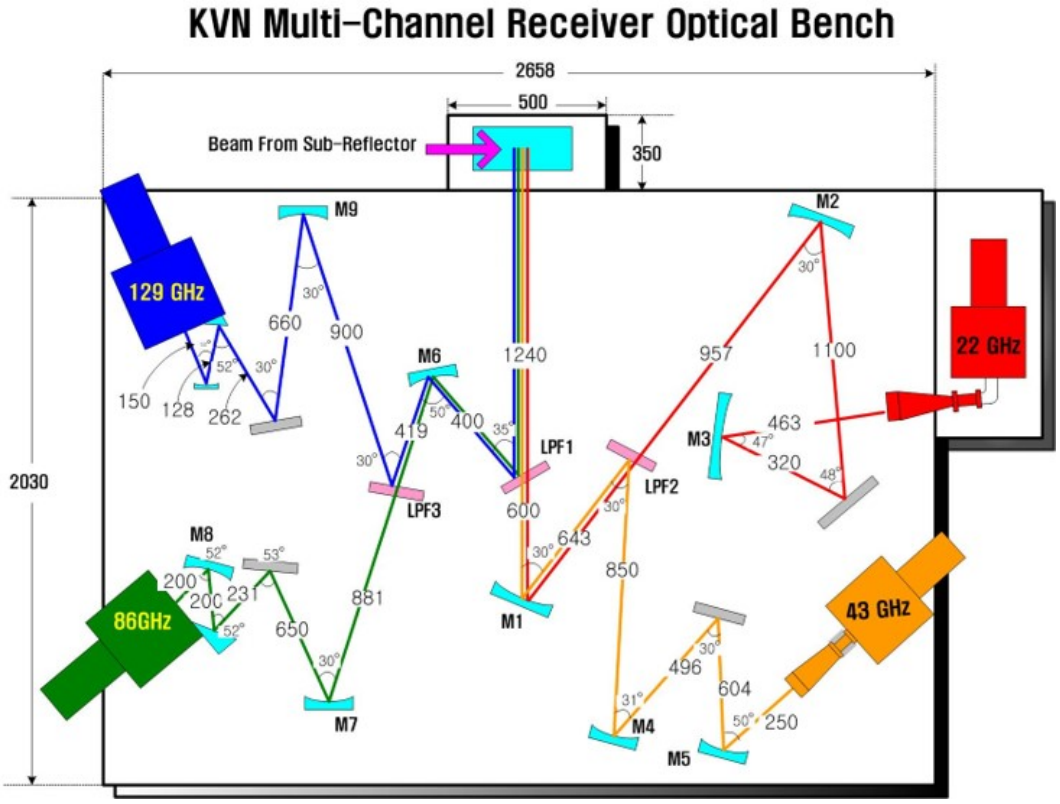

Figure 9: KVN multi-frequency receiving system.

observations until recently, with most of the testing finished. The receiving system of the KPC has been developed as an compact and wide-band receiver capable of simultaneous observations in the 18−230 GHz band. For the K, Q, and W bands, the CTR was designed and manufactured in-house to simultaneously observe them. To be more specific, the CTR system is mainly composed of a quasi-optical circuit, a cryogenic receiver, and a room temperature receiver system. The receiving frequency bands are divided into K (18–26 GHz), Q (35–50 GHz), and W band (80–116 GHz). These RF signals are then amplified and down-converted in the room temperature receiver, and finally converted into IF signals of 8–16 GHz. Additionally, it is possible to observe two polarization components (LCP and RCP) for each band simultaneously.

The quasi-optical circuit is a critical component that allows for simultaneous three-channel observations. It determines the antenna efficiency and receiver noise temperature, requiring complex design and high-quality assembly. Additionally, it necessitates sophisticated receiving beam alignment and precise measurement techniques. Cryogenic receiving systems are designed with a chamber that maintains a high vacuum and cryogenic temperature below 20 K. The chamber is equipped with a feed system that includes a cryogenic Low Noise Amplifier (LNA), feed horn, phase shifter, and orthogonal mode transducer (OMT). These components play a crucial role in influencing the receiver's noise temperature and stability. The room temperature receiving system comprises a room temperature amplifier and a local oscillator (LO) that convert the received RF signal to an intermediate frequency (IF). It also includes several band pass filters (BPFs), power divider, and mixers.

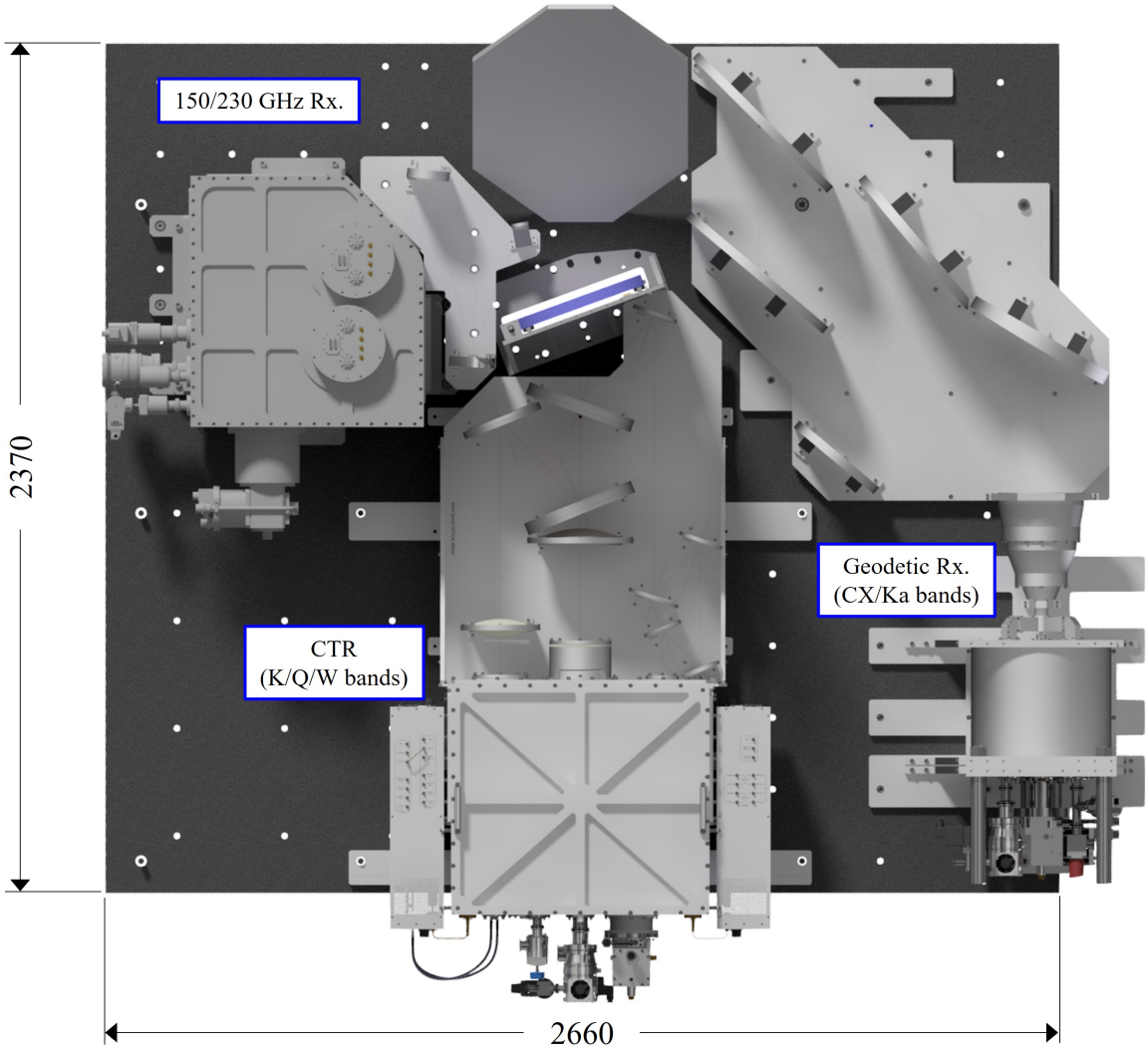

Figure 10: Layout of the KPC receiving system.

The CX/Ka band receivers were successfully installed on the KPC at the end of April 2025 and are currently undergoing a series of performance tests. Additionally, the 150/230 GHz receivers are scheduled for installation in 2025, with these receivers set to be utilized for research observations starting in 2026. Therefore, performance parameters for these receivers will be updated in next year's status report.

Figure 10 presents a layout of the KPC receivers, while Figure 11 shows a photograph of the receiver room as of May 2025, illustrating the installation of the CTR and CX/Ka band receivers.

2.3.2 Block diagram

The K, Q, and W band receivers are cooled HEMT receivers, while the D band receiver is an SIS mixer receiver [5]. All receivers are capable of receiving dual circular-polarization signals. Among eight signals (four dual-polarization signals), four signals selected by the

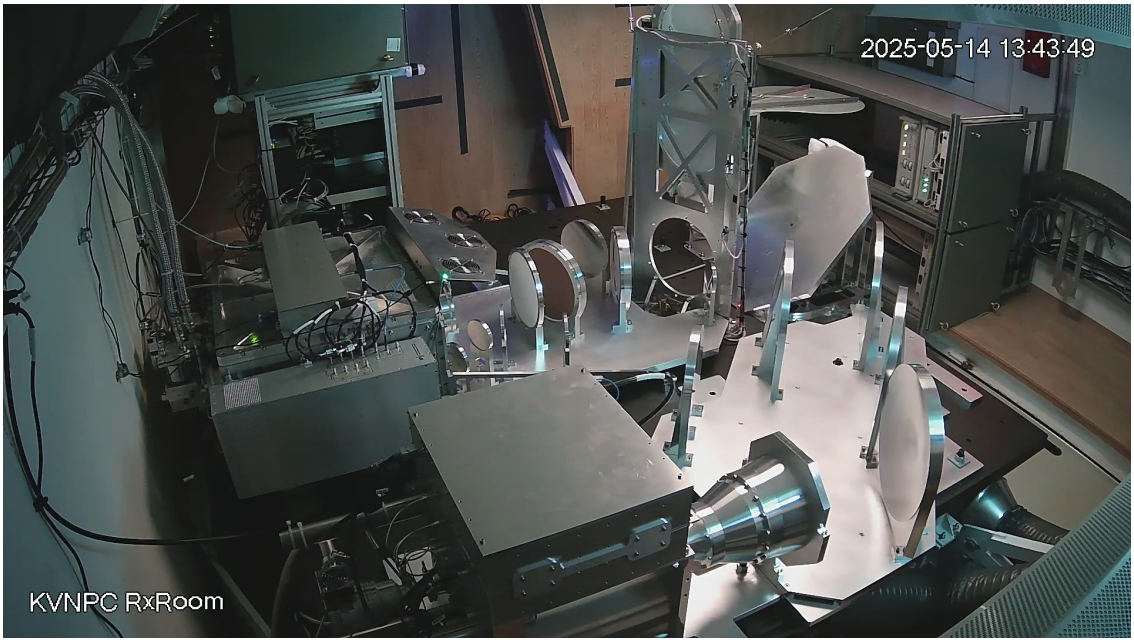

Figure 11: Receivers installed at KPC as of May 2025 (CTR + C/X/Ka band receivers).

IF selector are down-converted to the input frequency band of the sampler. The samplers digitize signals into 2-bit data streams with four quantization levels. The sampling rate is 1024 Mega samples per second, resulting in a 2 Gbps data rate (2-bit $\times$ 1024 megabytes per second) and 512 MHz frequency bandwidth. In total, we can get 4 streams of 512 MHz bandwidth (2 Gbps data rate) simultaneously, which means that the total rate is 8 Gbps.

New wide-band VLBI backends, including OCTAD, Mark 6, and GPU spectrometers, were installed for wide-band operation. They are indicated in the red box of Figure 12. The OCTAD consists of four analog-to-digital converters, digital signal processing modules, and a VDIF formatter. It digitizes four IF signals and performs signal processing for digital down-conversion and filtering. Combining OCTAD and ADS1K+Fila10G, all eight IF signals (four dual-polarization signals) can be obtained at the same time. The OCTAD has four 10 GbE outputs, with which we can get a maximum 32 Gbps aggregated data rate.

Furthermore, two wide-band VLBI sampler OCTADs and two GPU spectrometers were installed at KPC withe the objective of achieving enhanced performance in comparison to the original KVN system. As a result, the output rate of the KPC OCTAD can reach up to 64 Gbps. The details of the backend system, including OCTAD, are introduced in Section 2.4. The block diagram of receivers and backend interface of the KPC are illustrated in Figure 13.

2.3.3 Frequency range

The instantaneous bandwidth of the 1st IF of each receiver is limited to 8 GHz by the band-pass filter. Table 8 shows the frequency range of each receiver. The Q and W bands are divided into two frequency blocks. The low (high) frequency ranges of the Q band receiver are from 35 (42) to 42 (50) GHz. The low (high) frequency ranges of the W band

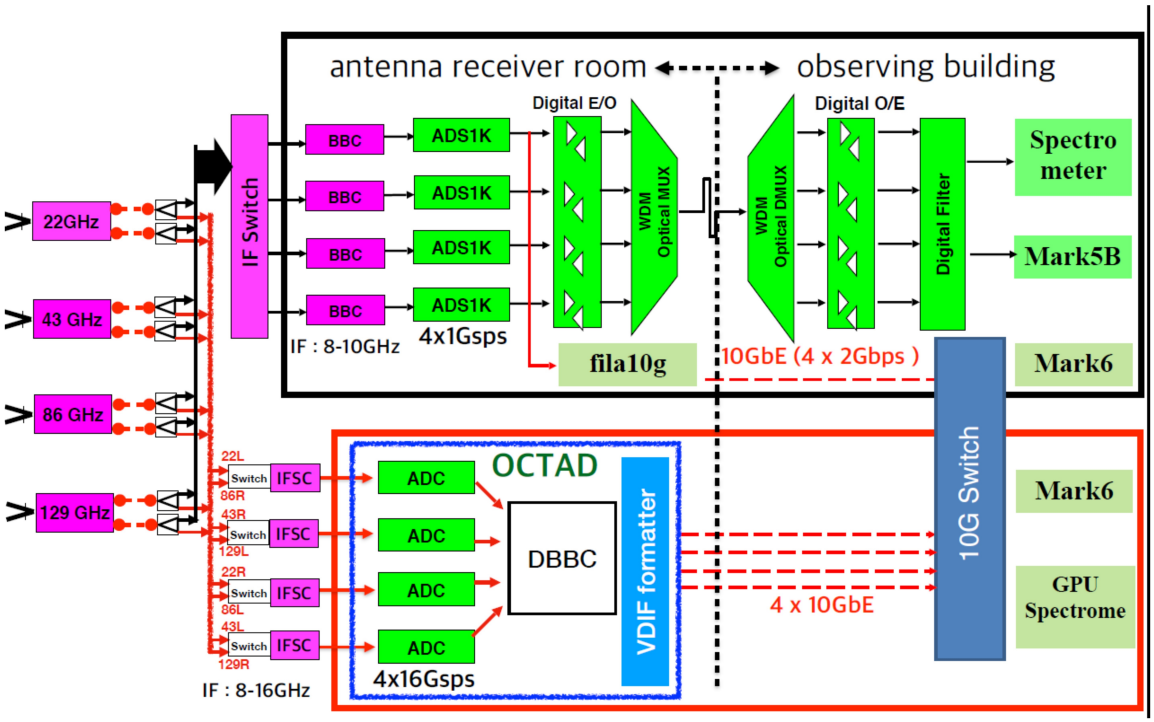

Figure 12: KVN signal flows including a new wide-band sampler OCTAD (from 2020).

receiver are from 85 (100) to 100 (116) GHz. Low- and high-frequency bands of the same polarization cannot be observed at the same time. Note that the D band receiver has 2 GHz IF bandwidth. The KPC with CTR system has slightly different frequency bands than the original KVN receivers. In the future, all original KVN receivers will be replaced with the CTR system.

Table 8: Frequency range of the KVN receiver

Band	Frequency range (GHz)	Telescope
CX	6 – 9	KUS, KPC
Ka	28 – 34	KPC
K	18 – 26	KYS, KUS, KTN, KPC
Q-low	35 – 43	KYS, KUS, KTN, KPC
Q-high	42 – 50	KYS, KUS, KTN, KPC
W-low	85 – 100	KYS, KUS, KTN
W-low	80 – 98	KPC
W-high	100 – 116	KYS, KUS, KTN
W-high	98 – 116	KPC
D	125 – 142	KYS, KUS, KTN
D-wide	125 – 170	KPC (in prep.)
sub-mm	210 – 275	KPC (in prep.)

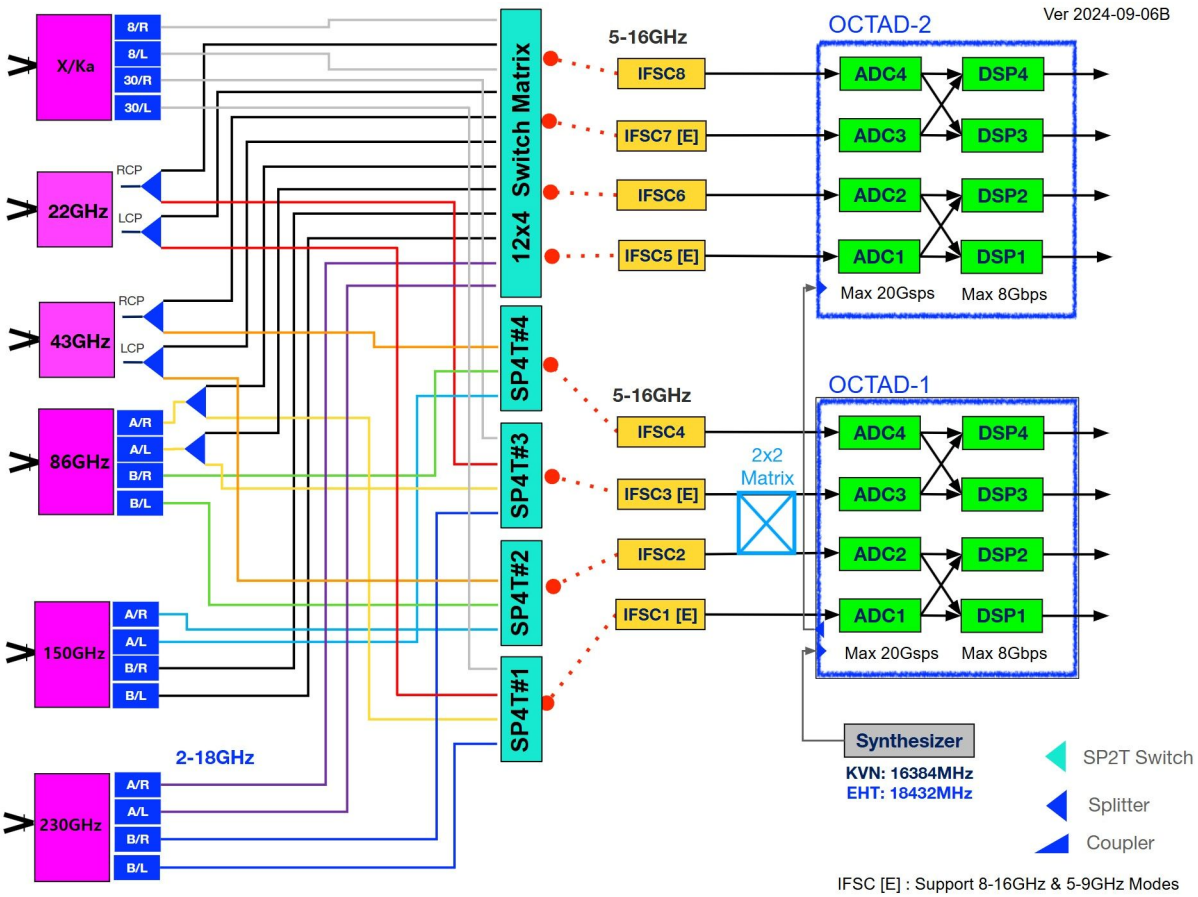

Figure 13: Block diagram of the signal connection between receivers and backend interface of the KPC.

2.3.4 Receiver noise temperature

Every frequency band has a receiver noise temperature that ranges from roughly 50 to 80 K. These values are similar for all bands. The loss of quasi-optics does not reduce the efficiency of the antenna aperture since the calibration chopper is placed before the quasi-optics; rather, it raises the temperature of the receiver noise. As a result, 40-–50 K are added to the noise temperatures to account for the quasi-optics losses.

2.3.5 System temperatures with wide-band frequencies

Wide-band observations are now possible with the KVN thanks to the integration of the GPU spectrometer and a new backend (OCTAD). In this regard, we evaluated the system temperatures over all wide-band frequency ranges, and the results are presented in Table 9. As a sample result, Figure 14 shows the system temperatures measured for the KTN's wide-band receiver system.

Table 9: System temperatures ($T_{\rm sys}$) using wide-band frequencies

Site	Band	Freq. range (GHz)	$T_{\rm sys}$ (K)	El. (degree)	Date
KYS	K	18 – 26	82 – 98	45 – 49	Jan. 17, 2023
	Q-low	35 – 42	60 – 112	51 – 52	Jan. 17, 2023
	Q-high	43 – 50	91 – 140	45 – 48	Jan. 17, 2023
	W-low	85 – 100	147 – 191	59 – 65	Jan. 27, 2023
	W-high	101 – 116	131 – 255	40 – 43	Feb. 01, 2023
	D	125 – 142	139 – 180	35 – 51	Jan. 27, 2023
KUS	K	18 – 26	71 – 91	55 – 56	Feb. 08, 2023
	Q-low	35 – 42	51 – 118	51 – 52	Feb. 08, 2023
	Q-high	43 – 50	85 – 156	46 – 48	Feb. 08, 2023
	W-low	85 – 100	153 – 203	48 – 61	Feb. 08, 2023
	W-high	101 – 116	150 – 315	43 – 61	Feb. 10, 2023
	D	125 – 142	145 – 279	36 – 46	Feb. 08, 2023
KTN	K	18 – 26	80 – 110	59 – 62	Nov. 10, 2024
	Q-low	35 – 42	46 – 114	49 – 58	Oct. 15, 2024
	Q-high	43 – 50	83 – 240	58 – 59	Oct. 15, 2024
	W-low	85 – 100	150 – 310	59 – 65	Oct. 19, 2024
	W-high	101 – 116	175 – 320	57 – 63	Oct. 20, 2024
	D	125 – 142	300 – 420	37 – 48	Oct. 27, 2024
KPC	K	18 – 26	54 – 83	34 – 62	Apr. 30, 2025
	Q-low	35 – 42	54 – 100	66 – 74	Apr. 30, 2025
	Q-high	43 – 50	101 – 200	51 – 58	Apr. 30, 2025
	W-low	80 – 97	148 – 191	34 – 64	May 02, 2025
	W-high	98 – 116	117 – 450	43 – 70	May 12, 2025

2.4 Backend/Digital Process

The KVN backend comprises a (wide-band) sampler that converts the IF signal from the receiver into a digital signal and a (wide-band) high-speed recorder that transfers the signal from the sampler to the hard disk. The KVN currently employs two modes: DAS system and OCTAD, a wide-band VLBI sampler.

2.4.1 Digital filter mode in DAS

The digital filter bank (DFB) is configurable to various modes according to the required number of streams and bandwidths. The DFB enables us to select in frequency domain 16 data streams of 16 MHz bandwidth from 4 streams of 512 MHz bandwidth. The corresponding data rate of the 16×16 MHz stream is 1024 Mbps, which corresponds to the maximum input data rate of the Mark5b recorder. Combining more than one stream, the DFB can produce streams with wider bandwidth such as 8×32 MHz, 4×64 MHz, 2×128 MHz, and 1×256 MHz (see Table 10).

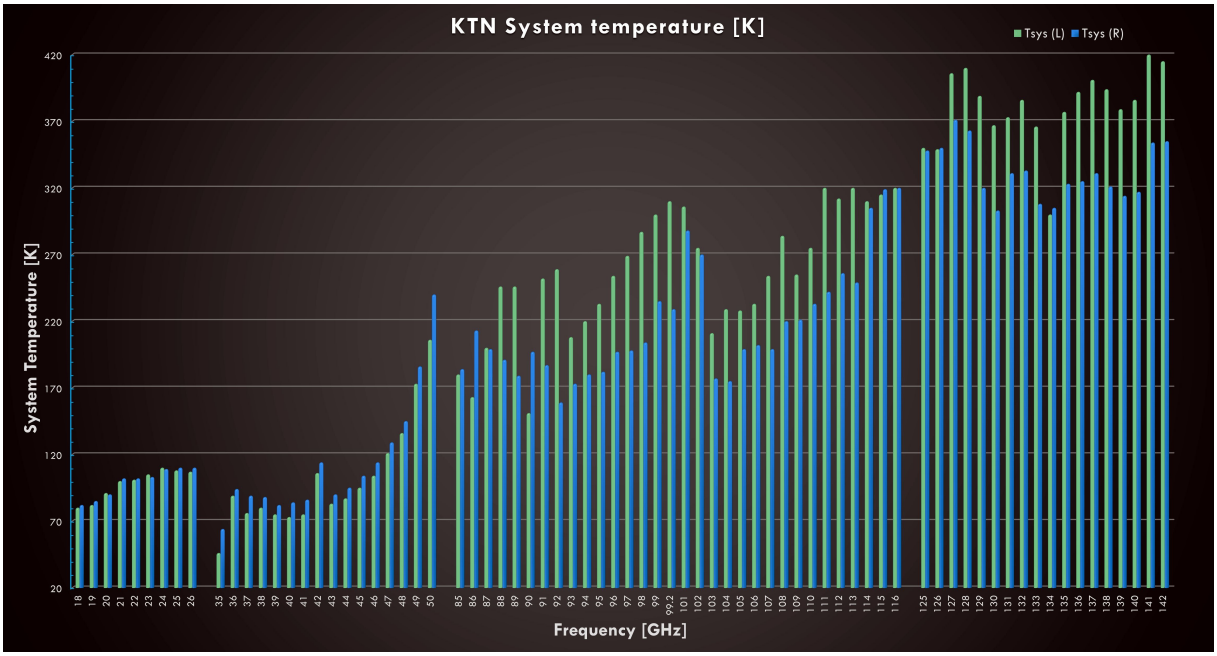

Figure 14: System temperatures with all wide-band frequencies of the KTN.

Table 10: KVN digital filter mode

Bandwidth (MHz)	Number of streams
16	16
32	8
64	4
128	2
256	1

A center frequency of a data stream is given by BW·(0.5 + N), where BW and N represent a bandwidth of data stream and integer number, respectively. If N is an even number, the data stream is the upper side-band. Otherwise, the data stream is in the lower side-band. Therefore, adjacent data streams have opposite side-bands. The center frequency cannot exceed 512 MHz.

2.4.2 Signal processing mode of OCTAD

The OCTAD (Optically Connected Transmission system for Analog to Digital Conversion) is the world's fastest sampler. It accepts analog signals with a maximum frequency of 24 GHz, quantized them to a resolution of up to 3 bits, and generates digital output data transmitted over fiber optic cables. Each unit has a standard data transfer capability of 10 Gigabit Ethernet (GbE). As illustrated in Figure 15, the OCTAD can accommodate up to four analog input ports. Since all four analog ports undergo identical processing, the following description focuses on the standard case of a single analog input.

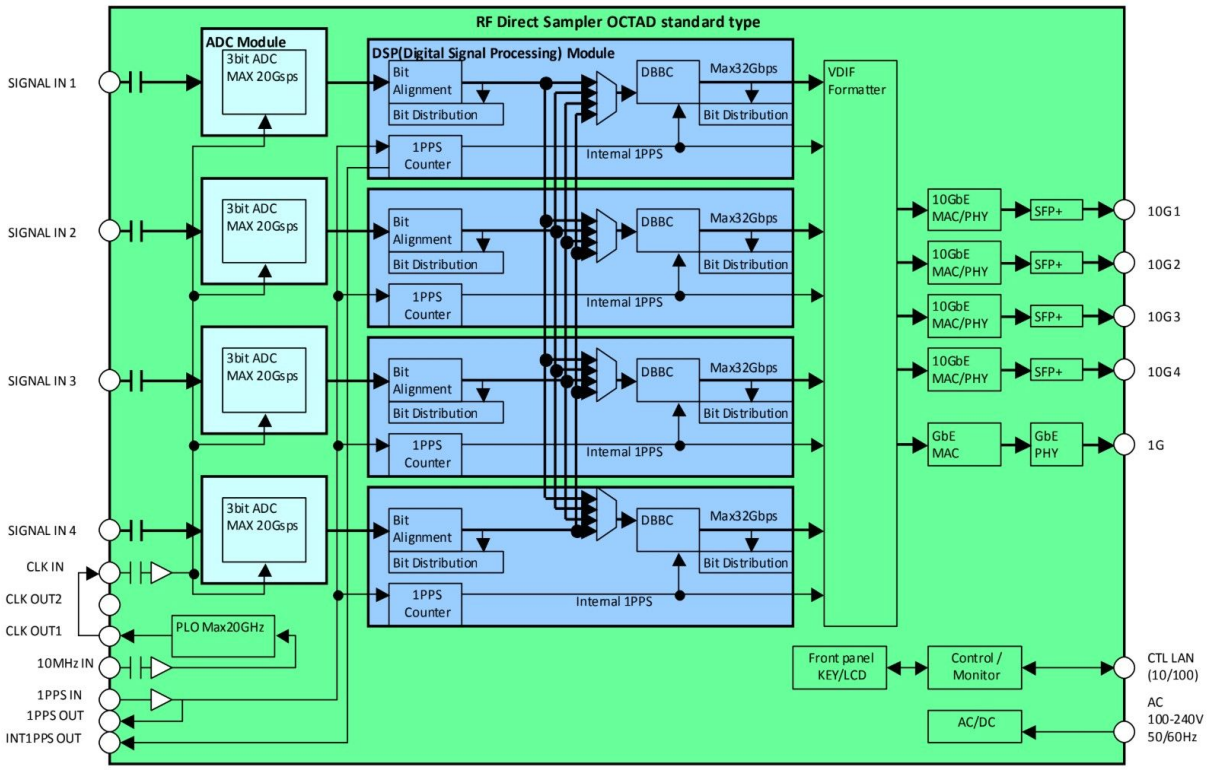

Figure 15: Functional Block diagram of the OCTAD

In the first, the analog input signal is quantized into eight levels using 3-bits within the box indicated as 'ADC'. The ADC operates with a quantization rate of up to 20 GHz. After quantization, the 3-bit data is de-multiplexed by one-to-two before being transmitted to the Signal Processing Module. The output data rate is approximately twice as slow, with a quantization of 10 GHz for 20 GHz. The ADC is followed by the Signal Processing Module, which consists of an FPGA, or Field Programmable Gate Array. The functions of 'Bit Alignment', 'Multiplexing', 'DBBC', 'Bit Distribution', and '1-PPS Counter' are implemented in the FPGA. The 'Bit Distribution' is a statistical analysis of sampled data. This function is an essential tool for verifying the input level of an analog signal. If the input analog signal is too weak, the occurrence of the code of '011' or '100' becomes very high, much higher than 19 % and the occurrence of other codes becomes very low, much lower than 15 % for '010' or '101' and 7 % for '000' or '111'.

The Bit Distribution is useful for two things. First, it can be used to check analog input levels. Second, it can be used to determine DC balance. For instance, if we fail to achieve a satisfactory DC balance, it becomes challenging to maintain an equal probability of occurrence for '100' and '011', the codes designated for negative and positive inputs, respectively. A "DBBC" is a digital base-band converter. It consists of a multiplier, a numerically controlled oscillator (NCO), and a digital filter (DF). The DBBC combines these functions to produce a data stream of signals, with each signal having a bandwidth of b.

The KVN telescopes are currently equipped with a single OCTAD each. However, there

Table 11: KVN OCTAD mode

Bandwidth (MHz)	Max. Number of streams	Total data rate (Gbps)
16	16	1
32	16	2
64	16	4
128	16	8
256	16	16
512	16	32
1024	8	32
2048	4	32

are plans to enhance their capabilities by adding another OCTAD for each telescope in the future, thereby increasing the total to two OCTADs per telescope. In current state, the OCTAD enables us to select in the frequency domain a maximum of 16 data streams from 4 streams of 8192 MHz bandwidth. The maximum output rate is 32 Gbps (4×8 Gbps) of which the net bandwidth is 8 GHz (4×2 GHz bandwidth). The total aggregated bit rate, number of streams, and bandwidths are specified in Table 11. The output data stream from the signal processing unit is routed to the VDIF formatter, which converts the output of the DBBC to the specified data format. The final formatted data are then converted to optical data and transmitted to the recorder unit using a standard communication protocol called 10 GbE.

Meanwhile, as mentioned above, the KPC is outfitted with two OCTADs, while the original KVN telescopes were equipped one DAS and one OCTAD systems. As a result, the maximum output rate of the KPC reach 64 Gbps, which corresponds to an 8 GHz bandwidth for 2-bit sampled data. Notably, this enhancement aligns the KPC with the observing mode specifications (2 GHz $\times$ 2 IF $\times$ 2 pol.) of the Event Horizon Telescope (EHT).

2.4.3 Recorders

The KVN station currently uses two main recording systems: the Mark6 and the Flexbuff. KUS also uses the Mark5b system for EAVN 6.7 GHz observations.

Mark5b and Mark6 are hard disk recording systems developed at Haystack Observatory, USA. The maximum data rate of Mark5b and Mark6 systems is 1 Gbps and 16 Gbps, respectively. For more details, see Haystack-memo-MK5b and Haystack-memo-MK6. At KVN stations, the Mark5b records the output data stream of a digital filter. Refer to section 2.3.2 for data stream connection and section 2.4.1 for available bandwidth and number of channels of 1 Gbps data stream.

The Mark6 records the OCTAD and Fila10G outputs in VDIF (VLBI Data Interchange Format). As the Fila10G has no digital filtering function, it can support up to four VSI streams, each with a bandwidth of 512 MHz. In contrast, the OCTAD offers greater flexibility in terms of IF numbers and bandwidth. For observations with a recording rate higher than 16 Gbps, KVN uses Flexbuff.

From 2023, we adopted **Flexbuff**, a system for recording VLBI data at super high speeds,

Figure 16: Front view of the two Flexbuff units at KPC. 24 disks are mounted for one Flexbuff.

developed by JIVE and proven for its performance and reliability by EVN and other networks (Figure 16). The Flexbuff system consists of a single host-based hardware that integrates more than 32 HDD arrays and storage servers to store high volume and high bandwidth files, and software that supports data recording at 32 Gbps. In the absence of dedicated hardware to produce the Flexbuff, the KVN chose PCI-E 4.0, 3rd generation CPU to handle the four 8 Gbps streams output from the OCTAD in real time. The Flexbuff platform of the "Supermicro" model has been installed at all KVN sites, including the KPC site. Additionally, **jive5ab**, a copy manager software designed for recording and transmitting VLBI data, based on the Linux OS "Rocky" has also been installed.

2.4.4 Spectrometers for Single-dish observation

- **Digital spectrometer**
  The VSI output data from the digital filter with an aggregation rate of 1024 MHz (256 MHz bandwidth) is processed using an FX-type digital spectrometer (DSM). The DSM is capable of processing 4 VSI streams that are sent from samplers via optical transmission. It processes data with a bandwidth of 4×512 MHz. It is capable of generating both cross- and auto-power spectrum data. For the purpose of observing polarization, cross-power spectrum measurements are employed. In all modes, the total number of FFT points accessible is set at 4096 channels per stream.

Table 12: Available mode of the GPU spectrometer (GSM)

Bandwidth (MHz)	Number of streams	Total data rate (Gbps)
32	16	2
64	16	4
128	16	8
256	8	8
512	4	8
1024	2	8
2048	1	8

- **GPU Spectrometer**
  The GPU spectrometer (GSM) processes VDIF data streams from OCTAD to create a power spectrum using FFT computations. The modalities that are accessible vary depending on the performance of the GPU cards and the host server of the GSM in each station. Table 12 provides a summary of them. Because of its considerable flexibility, the GSM can accommodate various numbers of FFT points. In a 32 MHz stream, we can obtain at least 4096 FFT points. As with a DSM, the GSM can generate both auto- and cross-power spectrum data. The single-dish polarization observations are not only valuable for the results obtained from single-dish observations, but they also serve as a crucial component for calibrating polarization angles in VLBI. Accordingly, a polarization observation mode of the KVN was developed using the wide-band backend system OCTAD and a GSM. Figure 17 shows the sample results of polarization observations for Mars and the Crab Nebula, respectively. This allows modes that use the new backend, OCTAD/GSM, to replace polarization observations with a single-dish using the previous backend, DAS/DSM. We can now observe polarization in frequency bands that the previous backend was unable to support thanks to the OCTAD's wide-band output, which also increases sensitivity.

2.4.5 Correlator

- **Daejeon Correlator in KJCC**
  KJCC(Korea-Japan Correlation Center) gathers the raw VLBI observation data from each site of KVN, VERA/JVN, and CVN, and performs the correlation process with two VLBI correlators. The first one, Daejeon Correlator, is one of the fastest VLBI correlators in the world and is used for processing the KaVA and EAVN observations mainly. It is capable to correlate the data streams of max. 8 Gbps for max. 16 stations in one pass, to produce the correlated output of 8192 spectral points for each sub-bands. The number of spectral points is reduced to 128 for continuum, 512 for line observation after the correlation process by channel integration.

  For the final correlation output, the default accumulation time is 1.6384 seconds and the final frequency resolutions are 16–128 MHz for continuum observations, and 16–512 MHz for line observations in default.

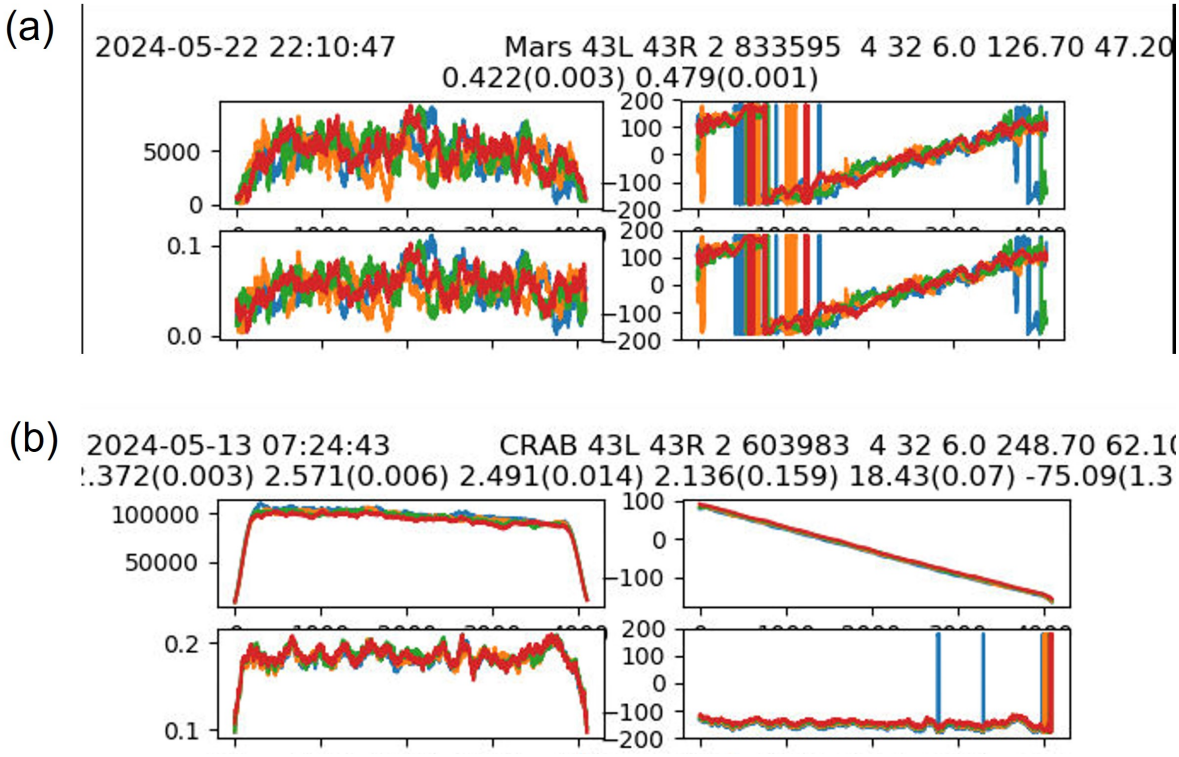

Figure 17: (a) The spectral result of a planet 'Mars' for calibration of polarization (left: amplitude, right: phase): Column 1 and 2 show the measurement and D-term, respectively. (b) Spectra of the polarization angle-corrected source 'CRAB' utilizing GSM (left, right: same as above): column 1 and 2 show the measured values and the linear polarization results.

The KJCC is currently able to support the following correlation modes (see Table 13).

The KJCC supports the following number of frequency channels for preparing FITS file.

Table 13: Correlation mode of the KJCC

Obs. Mode	Total Data Rate	Bandwidth /sub-band	# of sub-bands	Minimum Accum. Time	# of Freq. Channels /sub-band
C5	1024 Mbps	16 MHz	16	1.6384 sec	8192
C4	1024 Mbps	32 MHz	8	0.8192 sec	8192
C3	1024 Mbps	64 MHz	4	0.4096 sec	8192
C2	1024 Mbps	128 MHz	2	0.2048 sec	8192
C1	1024 Mbps	256 MHz	1	0.1024 sec	8192
W1	2048 Mbps	512 MHz	1	0.0512 sec	8192
W2	4096 Mbps	512 MHz	2	0.0512 sec	8192
W4	8192 Mbps	512 MHz	4	0.0512 sec	8192

- Basic output channel of correlator: 8192 frequency channel
- Continuum: 128 frequency channel (64 channels integrated in post-correlation)
- Spectral line: 512 frequency channel (16 channels integrated in post-correlation)

Correlation processing will take about 1 week to prepare the first version of FITS after the data arrives from the last station. However, the KJCC team will do their best to make correlation results available as quickly as possible to deliver the FITS file to PI. For more details, please see the webpage KJCC.

- **Software Correlator, DiFX**
The second one, DiFX (Distributed FX-style) software correlator (see Deller et al. (2007 [6], 2011 [7]), is the world-famous software correlator and is used for processing the KVN observations. It provides quite flexible correlation modes. You can request the accumulation time and the frequency resolution appropriate for your science purpose.

  A dedicated computing cluster named "Coma" for software correlation was installed. It is composed of one master and eight computing nodes. The master node has 128 GB of memory and two Intel Xeon E5−2667 v3 processors. Each of the processors has eight cores. Each computing node has 128 GB of memory and two Intel Xeon E5−2698 v4 processors. Each of the processors has 20 cores. The master and computer nodes are connected with 100 Gbps Infiniband and 1 Gbps Ethernet. The Infiniband connection is for parallel computation and storage, and the Ethernet connection is for management. OpenHPC has been used to deploy and manage the Coma cluster. A dedicated Lustre file system for the software correlation provides about 3 petabytes. It is connected to the master and each computing node through 100 Gbps Infiniband.

  Observation data saved in Mark5b or Mar6 at each KVN site is transported to the Luster file system through the KREONET using GridFTP. The master node has an additional 100 Gbps Ethernet connection to the KREONET. The KYS site is connected to the KREONET using 40 Gbps Ethernet, and the KUS and KTN sites are connected using 10 Gbps. Figure 18 shows the Coma computing cluster and the Lustre file system. Technical details of the software correlator are described in the homepage DiFX.

- **FITS delivery**
Correlations will be done using either the DiFX or the Daejeon correlator. The KJCC will deliver the FITS file to PI by using an FTP server or mobile disk.

  - When the correlation is completed, the FITS file will be prepared by post processing, and then the KJCC will announce the completion of the correlation processing to the PI by e-mail. In the e-mail, PI will be able to get the FITS file via a temporary URL link.
  - The PI should download the FITS file as soon as possible and check the FITS file using his or her preferred analysis tool. And then the PI should give his response to KJCC with "Success" (data quality is good) or "Fail" (download fail, bad FITS file, data quality is bad, etc.). Especially in the case of the "Fail" opinion, please send the error message to the KJCC, Your quick response for the FITS will be helpful for the KJCC to solve the problem as soon as possible.

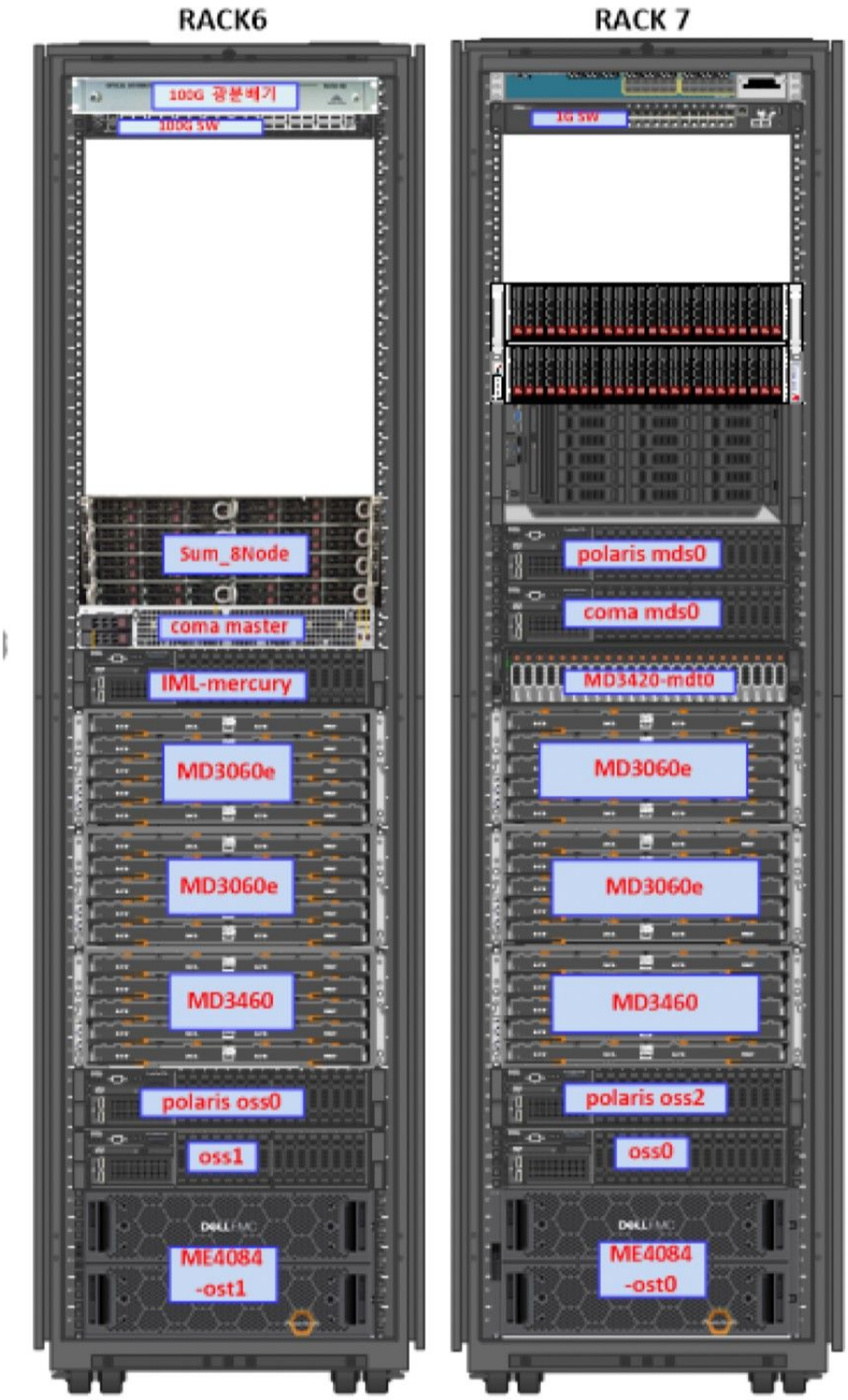

Figure 18: A computing cluster and Lustre file system dedicated for the software correlation of the KVN.

- The KJCC would like to receive PI's response within 2 weeks after announcing the email. If there is no response within 4 weeks, the KJCC determines that the PI's response is regarded as "success".
- In case of "Fail", according to the fail type, the KJCC will conduct the URL check, file reconstruction, or re-correlation, and then an announcement will be sent again to PI via e-mail.
- In the case of "Success", correlation processing for that observation will be closed (at that time, the download link in the temporary URL will be unavailable), and the tapes or disk modules will be included in the release pool for recycling.
- The FITS file provided to PI will be stored separately at the observation data archive. The PI should analyze, perform the research, and publish the paper within some period of time (in general, 18 months). After 18 months, the FITS file stored in the archive system will be opened to the public, who will need to do their research using that FITS according to the procedures.

- **Archiving policy**
  The KJCC organizes the archiving policy for observation data, CODA, and FITS files as below.
  - All VLBI data obtained with the KVN are accessible for collaborative purposes and will be utilized solely by the PI without external sharing until 18 months post-observation. After this exclusivity period, all data will be stored on KASI's dedicated servers and made publicly available through the Science Data Portal (http://data.kasi.re.kr, see Figure 19).
  - CODA: If correlated data is used for astrometry or geodesy, it is permanently stored at the CODA server. Otherwise, the correlated raw data and CODA file system will be deleted after receiving the response from PI.
  - FITS: it is permanently archived at the Archiving server.

2.5 Calibration for VLBI observations

System temperatures in Kelvin ($T_{\rm sys}$) are measured during observations at KVN stations once every user-specified interval (default 10 sec) to calibrate amplitude variation in time due mainly to atmospheric fluctuation. The measured $T_{\rm sys}$ is a sum of three temperatures: the receiver temperature, the spillover temperature, and the contribution of the atmosphere as described in Petrov et al. (2012) [8]. These $T_{\rm sys}$ values can be converted to SEFD (System Equivalent Flux Density) by dividing by the KVN antenna gains in K/Jy. The elevation dependence of the antenna gains is also corrected based on the normalized gain curves with lease-squared-fitted second-order polynomials as mentioned in previous Section 2.2.2.

Additional amplitude correction for the atmospheric opacity above an antenna is performed by conducting a sky tipping curve analysis according to the method described in Mangum (2000). In practice, the system temperatures ($T^*_{\rm sys}$) corrected for the atmospheric opacity are estimated based on the sky tipping curve measurements once every user-specified

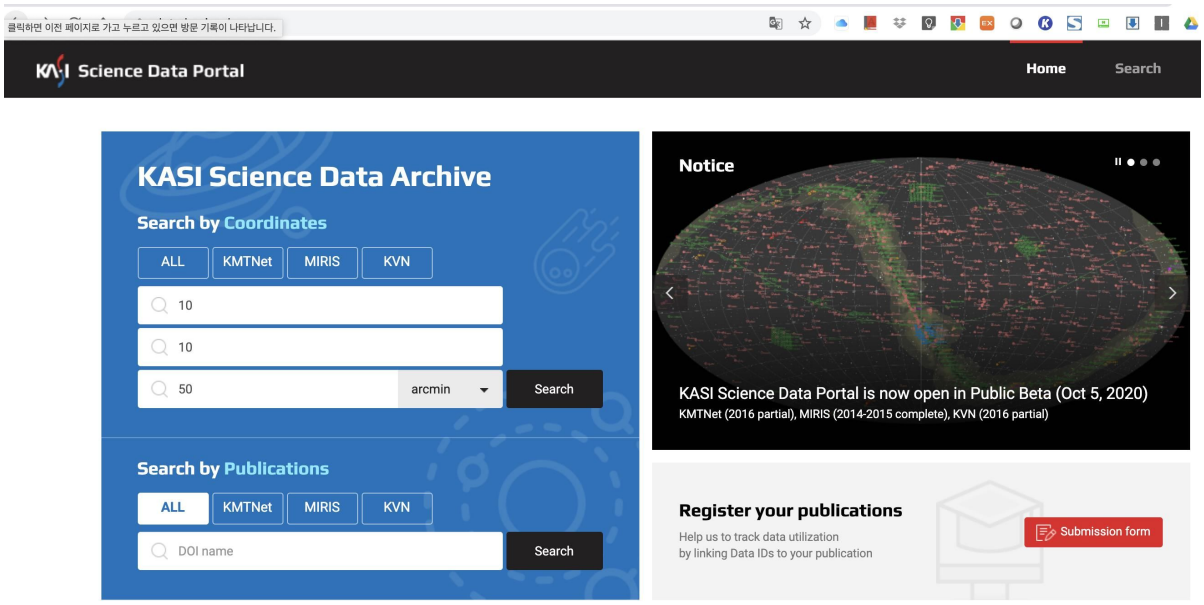

Figure 19: Initial screen of the KASI Science Data Portal

interval (default before and after an experiment). Further corrections are made to the KVN observations taken with 2-bit (4-level) sampling, for the systematic effects of the non-optimal setting of the quantizer voltage thresholds.

The amplitude calibrations with the KVN are accurate to 15 % or better at 22 and 43 GHz. However, it is recommended to observe a few amplitude calibrators during the scheduled observation time, allowing for (a) the assessment of the relative gains of KVN antennas and gain differences between IF-bands at each station, and (b) the confirmation of the correlation coefficient correction assuming that you have contemporaneous source flux densities obtained with other VLBI networks independent of the KVN observations.

2.6 KVN geodetic VLBI measurement

Obtaining accurate antenna positions is important in the VLBI system, especially for high precision astrometry. KVN antenna positions are regularly monitored using GPS and geodetic VLBI observations. The K band geodesy VLBI program between KVN and VERA started in 2011. Current KVN antenna positions (see Figure 20) were obtained from the KaVA K band geodesy on January 24, 2014. The typical 1-sigma errors of geodetic solutions are about 0.4 cm in the X, Y, and Z directions. Based on 22-epoch KaVA K band geodetic observations from September 2012 to December 2016, uncertainties of KVN antenna positions are $\sim$ 2.38 cm at KYS, $\sim$ 2.55 cm at KUS, and $\sim$ 1.58 cm at KTN.

The accurate positions of the KVN antennas were recently derived from IVP measurements using GNSS. These are described in Section 2.1.3.

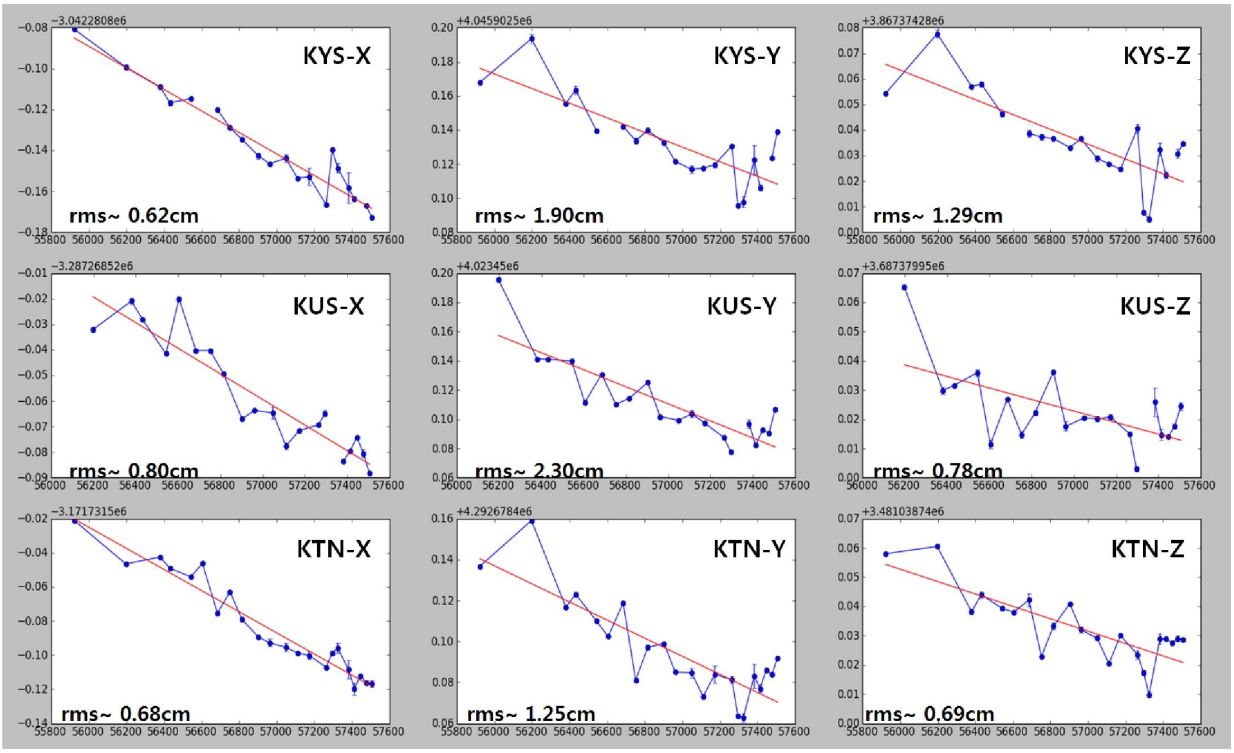

Figure 20: The trend of KVN antenna positions (IVP) in the ITRF 2014 coordinate system. The x and y axes are MJD and X, Y, and Z in meters. The linear fitting is applied to the measurements, shown as red line, and its deviation is also presented in each axis as "rms".

3 Observing proposal

3.1 Observing mode

3.1.1 Multi-frequency observation

Simultaneous multi-frequency observation is a unique capability of the KVN, with which we can calibrate out the short-term phase fluctuations at higher frequency data by referencing the phase solution obtained from lower frequency data. This phase referencing technique allows us to integrate the data for a time scale much longer than the coherent time scale of atmospheric phase fluctuation and so to observe weak sources at mm-wavelength efficiently. For multi-frequency observations, we can select no more than 4 IFs among 8 IF signals (= 4 receivers × 2 polarizations). The observation technique for a simultaneous multi-frequency observation can be summarized by a formula as shown in Figure 21.

3.1.2 Fast position switching observation

The slewing speed and acceleration rate of the KVN antenna are 3 °/sec and 3 °/sec^2, respectively. Due to this high speed and acceleration rate, the KVN antenna can switch its pointing from target to calibrator in a short period of time.

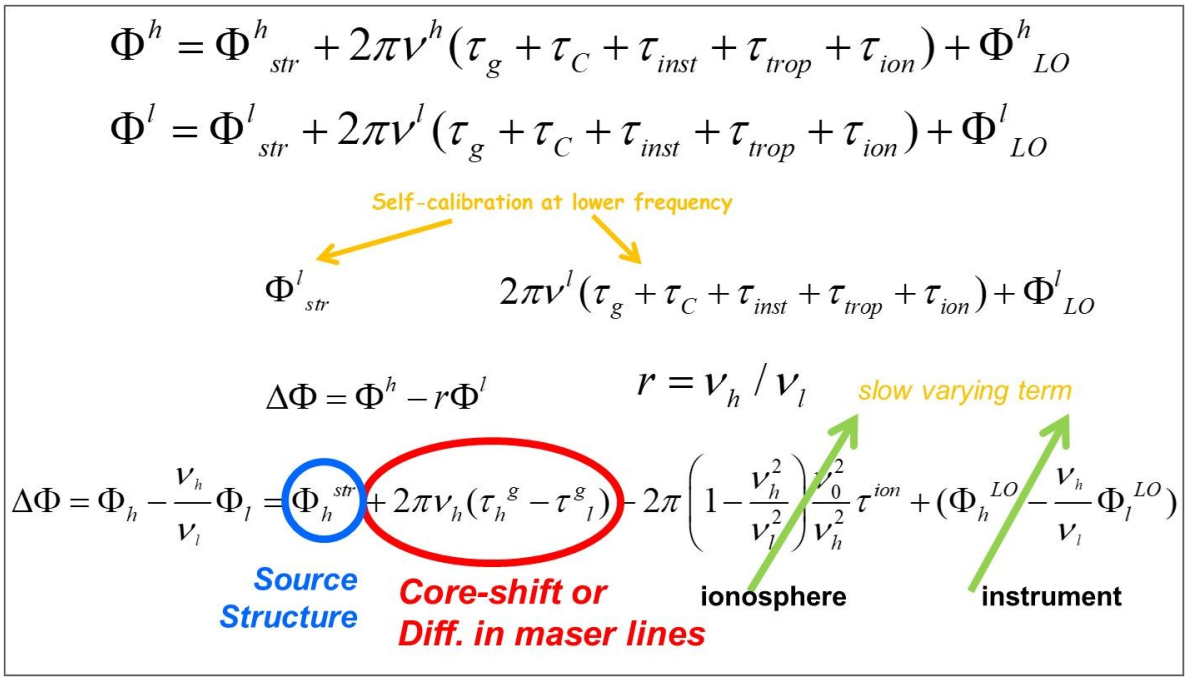

Figure 21: Scheme of Simultaneous Multi-frequency Calibration

3.1.3 Recording rate

2 Gbps (1×512 MHz), 4 Gbps (2×512 MHz), 8 Gbps (4×512 MHz) modes, which use fila10G and Mark6 recorders, have been fully evaluated in 2017. These modes are currently available for common use observations. For multi-frequency observations, we can select 1, 2, or 4 IFs among 8 IF signals (= 4 receivers × 2 polarizations). Furthermore, observations in 16 Gbps and 32 Gbps modes are now available following the installation of the high-speed recorder FlexBuff and the VLBI sampler OCTAD. These are explained with additional detail in Section 2.4 and are further addressed below.

- 16 Gbps mode
  - KYS, KUS, KTN: OCTAD (*8 Gbps) + 4 ADS1K + fila10G (8 Gbps: 512 MHz × 4 CH)
    *8 Gbps: 128 MHz × 16 CH, 256 MHz × 8 CH, 512 MHz × 4 CH
  - KPC: OCTAD1: 8 Gbps, OCTAD2: 512 MHz × 4 CH (4 Gbps)
- 32 Gbps mode (for Flexbuff)
  - 2048 MHz × 4 CH, 1024 MHz × 8 CH, 512 MHz × 16 CH

3.2 Angular resolution

Table 14 shows the maximum lengths (B) of the KVN baselines in km and the corresponding resolutions ($\theta_{\rm HPBW}$) in milli-arcsecond (mas), which is estimated as $\theta_{\rm HPBW}$ (mas) $\sim 20627 \cdot \lambda$(mm)/B(km).

Table 14: Angular resolutions at each KVN baseline and frequency

Baseline	B (km)	$\theta_{\rm HPBW}$ (mas)			
		22 GHz	43 GHz	86 GHz	129 GHz
KYS–KUS	305.0	9.1	4.7	2.4	1.6
KUS–KTN	358.8	7.8	4.0	2.0	1.3
KTN–KYS	478.0	5.8	3.0	1.5	1.0
KPC–KYS	133.1	20.9	10.8	5.4	3.6
KUS–KPC	232.6	12.0	6.2	3.1	2.0
KTN–KPC	505.8	5.5	2.9	1.4	0.9

3.3 Baseline sensitivity

Table 15 shows sensitivities of the KVN baselines as follow: (1) frequency band, (2) nominal frequency range of KVN receivers, (3) system temperature, (4) typical KVN system-equivalent-flux-density at zenith, (5) antenna gain at the optimal elevation, (6) typical KVN baseline sensitivity for the aggregated recorded data rate of 1024 Mbps, the integration time of 100 sec (K band), 60 sec (Q band), and 30 sec (W/D band), and the bandwidth of 256 MHz, and (7) typical KVN 3-baseline image sensitivity for the on-source integration time of 8 hr.

Table 15: Baseline sensitivity of the KVN

Freq. band	Freq. range (GHz)	$T_{\rm sys}$ (K)	SEFD (mJy)	Gain (K/Jy)	ΔS (mJy)	ΔI (mJy/beam)
(1)	(2)	(3)	(4)	(5)	(6)	(7)
K	21.25–23.25	100	1129	0.089	12	0.2
Q	43.11–44.11	150	1715	0.087	18	0.3
W	85–95	200	2073	0.072	29	0.6
D	125–142	250	3041	0.049	54	1.0

3.4 Support for International Multi-freq. VLBI Observations

The KVN telescopes are employed for active research observations in conjunction with the EAVN, EVN, and GMVA telescopes as part of an international collaborative observing network. Specifically, they serve as the primary axis of the EAVN. For more information on international joint observations, please refer to the EAVN Status Report. At present, the Yebes (Spain) and the Nobeyama (Japan) are equipped with receiving systems and backends for simultaneous K/Q/W band observations. The Italian telescopes–Notto, SRT, and Medicina–are in the process of upgrading their capabilities for W-band observations, utilizing CTR receivers developed and distributed by the KVN Center of the KASI. These telescopes are expected to be available for joint observations in 2026. According to the latest data, there are currently nine international telescopes (including the KVN & Sejong telescope) capable of conducting simultaneous K/Q band observations. Furthermore, six international telescopes (including the KVN telescopes) are capable of simultaneous K/Q/W

band multi-frequency observations. Looking ahead, we expect a significant increase in joint observational opportunities during the 2026–2027 period, particularly with the integration of the three Italian telescopes, as well as the German Effelsberg and Finnish Metsähovi telescopes.

4 Observation and Data Reduction

4.1 Preparation of observation and correlation

4.1.1 General information

For the accepted proposals, the users have to prepare the observing schedule file before the observation. The observer who is not familiar with the KVN system is recommended to consult contact persons of the KVN group to prepare schedules, especially for some observations such as phase referencing, polarimetry, and/or spectral line, etc. Comprehensive information regarding the observation planning and scheduling process is available on the KVN website[2].

4.1.2 Observation

All KVN experiments should be scheduled using the VEX (VLBI experiment) file. You can either edit and modify the KVN VEX example files or use the VLBA scheduling program SCHED[3]. It is recommended to use SCHED for your scheduling because SCHED provides useful information and many aspects of planning VLBI observations, and you can also avoid many mistakes arising from editing the VEX manually. The user needs to submit the VEX or key files two weeks before the observation. KVN AOC staff will check your schedule and proceed with the observations.

4.1.3 Correlation

Following the observation, the Daejeon correlator or DiFX correlator will perform the correlation procedure in accordance with the parameters that were provided. In order to release and recycle the disk modules and storage used for observation, the user is required to review the correlated data and report if the correlation was correctly performed. If there are any issues, re-correlation may be required. The raw data disk modules utilized for the observations will, in principle, be discarded two months after the correlation. Please see the correlation status report for further details.

[2] https://radio.kasi.re.kr/kvn/user_support.php
[3] http://www.aoc.nrao.edu/~cwalker/sched/sched.html

4.2 Data reduction

4.2.1 VLBI data reduction with AIPS

Here we introduce a very brief way of reducing VLBI data with KVN (or EAVN). For more detail, please have a look at the data reduction manual[4]. Figure 22 shows one of the procedures for reducing the KVN (or EAVN) observations.

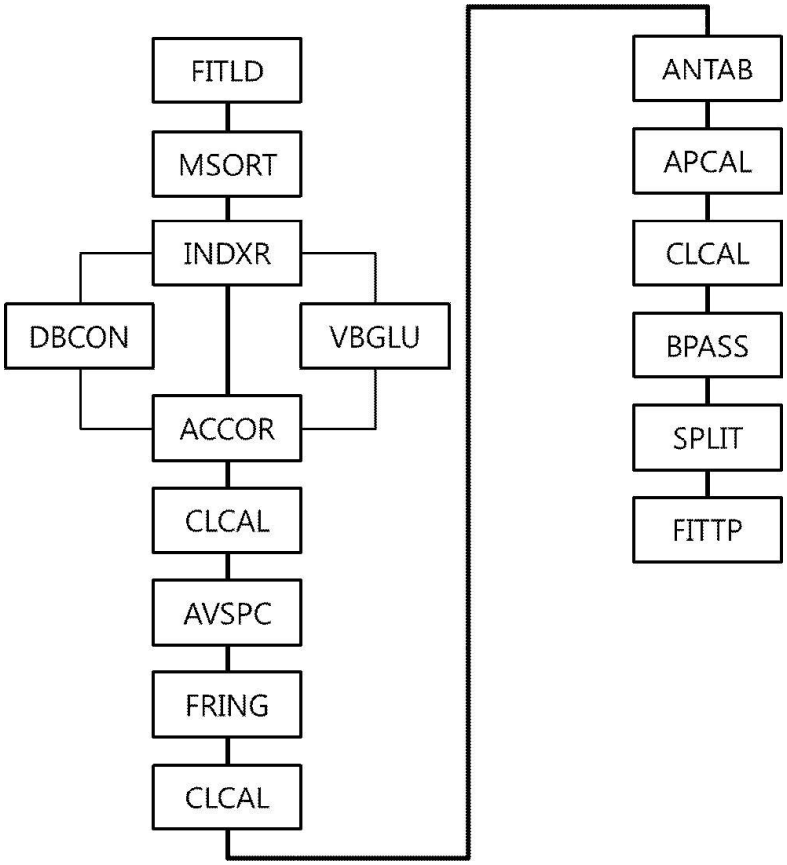

Figure 22: Data reduction flow chart with AIPS

5 Further information

Contact address It is possible for users to contact any staff member of the KVN by email (see Table 16). The official website[5] also provides various types of information.

[4] https://radio.kasi.re.kr/eavn/user_support.php
[5] http://kvn.kasi.re.kr

Table 16: Contact information

E-mail	Subject
kvnprop@kasi.re.kr	Proposal submission and informing its result
kvnobs@kasi.re.kr	Observing schedule submission, observation-related requests and questions for the accepted proposal only
kjcc@kasi.re.kr	Correlated data distribution and correlation-related requests
kvnhelp@kasi.re.kr	General questions including scheduling, observations, systems, and so on (regardless of the proposal acceptance)

References

[1] S.-S. Lee, L. Petrov, D.-Y. Byun, J. Kim, T. Jung, M.-G. Song, C. S. Oh, D.-G. Roh, D.-H. Je, S.-O. Wi, B. W. Sohn, S.-J. Oh, K.-T. Kim, J.-H. Yeom, M.-H. Chung, J. Kang, S.-T. Han, J.-W. Lee, B. G. Kim, H. Chung, H.-G. Kim, H. Ryoung Kim, Y.-W. Kang, and S.-H. Cho, "Early Science with the Korean VLBI Network: Evaluation of System Performance," The Astronomical Journal, vol. 147, p. 77, Apr. 2014.

[2] I. de Pater, R. J. Sault, M. H. Wong, L. N. Fletcher, D. DeBoer, and B. Butler, "Jupiter's ammonia distribution derived from VLA maps at 3-37 GHz," Icarus, vol. 322, pp. 168–191, Apr. 2019.

[3] M. Maris, E. Romelli, M. Tomasi, A. Gregorio, M. Sandri, S. Galeotta, D. Tavagnacco, M. Frailis, G. Maggio, and A. Zacchei, "Revised planet brightness temperatures using the Planck/LFI 2018 data release," Astronomy and Astrophysics, vol. 647, p. A104, Mar. 2021.

[4] S.-T. Han, J.-W. Lee, J. Kang, D.-H. Je, M.-H. Chung, S.-O. Wi, T. Sasao, and R. Wylde, "Millimeter-wave Receiver Optics for Korean VLBI Network," International Journal of Infrared and Millimeter Waves, vol. 29, pp. 69–78, Jan. 2008.

[5] S.-T. Han, J.-W. Lee, J. Kang, C.-S. Oh, D.-Y. Byun, D.-H. Je, M.-H. Chung, S.-O. Wi, M. Song, Y.-W. Kang, S.-S. Lee, S.-Y. Kim, T. Sasao, P. F. Goldsmith, and R. Wylde, "Korean VLBI Network Receiver Optics for Simultaneous Multifrequency Observation: Evaluation," Publications of the Astronomical Society of the Pacific, vol. 125, p. 539, May 2013.

[6] A. T. Deller, S. J. Tingay, M. Bailes, and C. West, "DiFX: A Software Correlator for Very Long Baseline Interferometry Using Multiprocessor Computing Environments," , vol. 119, pp. 318–336, Mar. 2007.

[7] A. T. Deller, W. F. Brisken, C. J. Phillips, J. Morgan, W. Alef, R. Cappallo, E. Middelberg, J. Romney, H. Rottmann, S. J. Tingay, and R. Wayth, "DiFX-2: A More Flexible, Efficient, Robust, and Powerful Software Correlator," , vol. 123, p. 275, Mar. 2011.

[8] L. Petrov, S.-S. Lee, J. Kim, T. Jung, J. Oh, B. W. Sohn, D.-Y. Byun, M.-H. Chung, D.-H. Je, S.-O. Wi, M.-G. Song, J. Kang, S.-T. Han, J.-W. Lee, B. G. Kim, H. Chung,

and H.-G. Kim, "Early Science with the Korean VLBI Network: The QCAL-1 43 GHz Calibrator Survey," The Astronomical Journal, vol. 144, p. 150, Nov. 2012.